Aerospace Science and Technology 120 (2022) 107252

Contents lists available at ScienceDirect

Aerospace Science and Technology

www.elsevier.com/locate/aescte

Adaptive distributed finite-time formation control for multi-UAVs under input saturation without collisions

Bojian Liu, Aijun Li, Yong Guo *, Changqing Wang

School of automation, Northwestern Polytechnical University, Xian 710072, China

ARTICLE INFO

Article history:
Received 27 January 2021
Received in revised form 11 October 2021
Accepted 26 November 2021
Available online 1 December 2021
Communicated by Xiande Fang

Keywords:
Finite-time control
Collision avoidance
Input saturation
Multi-UAVs
Backstepping control

ABSTRACT

This paper devotes to addressing the adaptive distributed finite-time formation control problem for multi-UAVs with collision avoidance and input saturation. By combining the formation reconstruction algorithm designed in this paper, the novel adaptive finite-time control law that utilizes the nonlinear mapping technology and prescribed performance control can limit the UAVs in the specified region to avoid collisions between each other. Moreover, an improved auxiliary dynamic system governed by hyperbolic functions is constructed to address the input saturation problem, while promoting to achieve the finite-time convergence of tracking errors. Finally, the convergence of the error systems and the practicability of the control law are verified by Lyapunov stability analysis and numerical simulations.

1. Introduction

After decades of development and application, the formation control of UAVs is relatively mature and plays a unique and irreplaceable role in both civilian and military aspects [1]. For example, in the civil field, UAV formation can be used for forest fire prevention [2], urban governance [3], environmental protection [4], and other tasks. In the military field, UAV formation can be employed for load transportation [5], target detection [6], and so on. The formation control methods can be divided into decentralized control, centralized control and distributed control. As a branch of formation control law, distributed control has unique advantages in both academic and engineering [7].

Recently, the distributed formation control has attracted intensive research attention for its small communication burden and clear logical relationship. It has been greatly developed with a reduced integral model in cooperative encirclement hunting [8], robotic formation [9], and other fields [10]. To further reduce the communication burden, distributed event-trigger-based controllers were proposed in [11, 12] with the communication constraints. Based on the intelligent pigeon behavior, a distributed control structure imitating the structure of the pigeon group was proposed [13,14]. Besides, some artificially intelligent scheme were used in distributed control and swarm of UAVs [15–17]. However, the biggest challenge with distributed control is that the followers do not know the status of the leader, which leads to errors that are transmitted step by step. To solve this problem, distributed observers came into being. Based on the linear model, distributed observer approach was widely used to make all followers obtain information about the leader [18,19]. Although there are a lot of advanced algorithms that have been proven to work well on simple models like multi-agents systems, it is still very difficult to apply them to complex models. Thus, more researchers focus on the formation problem of UAVs with consideration of the precise model. Based on the precise fixed-wing UAV model, an event-triggered-based formation control law was presented to reduce communication between UAVs in [20,21]. To deal with the unknown control direction, Nussbaum-based control law was constructed for UAVs [22,23]. Considering the actuator failures and unknown parameters problems introduced by the nonlinear dynamics, the radial basis function neural network (RBFNN) and disturbance observer were employed in [24–26] to design the distributed formation controller.

When researchers emphasize the nonlinear dynamics of UAVs, the input saturation problem deserves further study. Any actual system has its input limitation, and controller design without considering the input saturation will reduce its practicability. It may cause poor control effects or even divergence of the system. Therefore, the input saturation problem has recently become a research hotspot. By designing an intermediate control law, a novel input dynamic system was designed in an integral form that is skillfully constructed to

* Corresponding author.
E-mail address: guoyong@nwpu.edu.cn (Y. Guo).

https://doi.org/10.1016/j.ast.2021.107252
1270-9638/

generate the input signals that fulfill the saturation [27]. In [28], a compensation (auxiliary) system that has been widely used was designed to compensate the effect of the saturation, and its states are used to adaptive tracking control design. For the shortcomings in the compensation system that is not continuous and can not enforce the compensation function when input saturation reappears, Zhu [29] recently proposed an improved continuous system that can compensate input signal and achieve better results. Another approach to deal with input saturation is based on the mean value theorem and the adaptive approach [30,31]. The saturation nonlinearities are defined as the Gaussian error function [32] and the hyperbolic tangent function [33], which allows the input saturation problem can be addressed. Recently, the Nussbaum-type function–based method to handle the input saturation has got more attention, because it can also address the unknown direction control problem [22,23]. Nevertheless, the literature reviews mentioned earlier do not take collision avoidance into consideration, which is also an important issue in engineering applications.

Collision avoidance is quite necessary for formation control. If UAVs collide with each other during the flight, it will cause great damage to the completion of the mission. Thus, many scholars have great enthusiasm for collision avoidance algorithms. There are two main directions for collision avoidance, one is based on control law and the other is based on trajectory planning. The hottest method based on control law is the distance-based approach like artificial potential field (APF). There are many controllers that can achieve collision avoidance by combining the novel potential function [34,35]. However, they all have an obvious drawback is the existence of local minimums [36]. To avoid local minimums, many studies have been carried out like dynamic APF [20], novel types of APF [37,38] and the backtracking-filling method [39]. Although there are some methods to deal with the local minimums in APF, they all increase the complexity and difficulty of the control law design.

In recent years, with the advances of the prescribed performance algorithm, some works have been proposed to address the collision problem to avoid the disadvantage of APF. A distance-based formation control protocol with prescribed performance was proposed in [40] to ensure collision avoidance among the neighbor agents. Based on the leader-follower formation tracking control problem, the control laws were designed by the prescribed performance algorithm in [41], which can only ensure collision avoidance between the immediate leader and its follower. Therefore, considering the global collision avoidance, a formation control law by using a novel prescribed performance function for connectivity-preserving and collision-avoiding formation tracking was presented without employing any potential functions [42,43]. However, these controllers either failed to achieve global collision avoidance or required a lot of topology switchings.

By synthesizing the aforementioned observations, there are few pieces of research addressing the formation control for the precise model of the UAVs with collision avoidance. Thus, to enrich the relevant research, the two main novelties of the works in this paper are proposing a novel collision avoidance method and designing an improved auxiliary system to handle the input saturation problems introduced by the precise model of the UAVs. The novel collision avoidance method is composed of two parts. One is the formation reconstruction algorithm that can reasonably match the UAVs based on their current positions with the desired formation positions, which provides the collision avoidance area for the UAVs. The other is the novel Lyapunov function composed of the prescribed performance and the position error term that can limit the UAVs in the specified region to achieve collision avoidance during the flight. Besides, an improved auxiliary system to handle the input saturation problems is proposed in this paper, which compensates for the error caused by input saturation according to the virtual control input by increasing the system order. The main contributions of this work are listed as follows:

1. The distributed control scheme designed in this paper can achieve collision avoidance by limiting the flight space of the follower UAVs to a specified region. Combining with the novel Lyapunov function composed of the prescribed performance and the position error term, the control scheme can accomplish global collision avoidance with a simple structure.
2. The novel dynamic system to ensure that the control input satisfies the magnitude limits is proposed in this paper, which can address both the symmetric and asymmetric control saturation problem. Compared with the dynamic system proposed in [27], the dynamic system presented in this paper does not have the time-varying upper-bounded problem that will lead to insufficient input in the primary stage.

The rest of this paper is organized as follows. Section 2 presents the preliminaries, longitudinal model of UAVs, formation reconfiguration algorithm and RBFNN. Section 3 introduces the distributed finite-time formation controller design based on the backstepping method with the unknown dynamic parameters, collision avoidance and input saturation. Furthermore, the associated stability analyses are presented. Section 4 studies the simulation results of the proposed control law, which demonstrates the effectiveness of the method. Section 5 outlines the conclusions and future works.

2. Preliminaries and problem formulation

Throughout this paper, the following notations will be used. $\Re^{n\times m}$ and $\Re^n$ denote the sets of $n \times m$ real matrices and n-dimensional vectors respectively. $\|\bullet\|_2$ means the Euclidean norm. $sig^k(\bullet) = sign(\bullet)|\bullet|^k$ for $\bullet \in \Re$, where $sign(\bullet)$ is the sign function and $|\bullet|$ is the absolute value of $\bullet$. $x[k]$ denotes the kth element of the vector x, and $sig^k(x) = \left[sig^k(x[1]), sig^k(x[2]), \ldots, sig^k(x[n])\right]^T$ for $x \in \Re^n$.

Lemma 1 *([24]). Consider the system $\dot{x} = f(x)$. Suppose that there exists a continuous function $V(x)$, scalars $\lambda_1 > 0$, $\lambda_2 > 0$, $0 < a < 1$ and $0 < \eta < \infty$ such that*

$$\dot{V}(x) \le -\lambda_1 V(x) - \lambda_2 V^a(x) + \eta. \tag{1}$$

Then, the system state x converges into the bounded region $\Omega = \min\{\Omega_1, \Omega_2\}$ in a finite time $t = \max\left\{t_{f1}, t_{f2}\right\}$ where $t_{f1} \le 1/\vartheta\lambda_1(1-a)\ln\left(\vartheta\lambda_1 V^{1-a}(x(0)) + \lambda_2\right)/\lambda_2$, $t_{f2} \le 1/\lambda_1(1-a)\ln\left(\lambda_1 V^{1-a}(x(0)) + \vartheta\lambda_2\right)/\vartheta\lambda_2$, $\Omega_1 = \{x : V(x) \le (\eta/(1-\vartheta)\lambda_1)\}$ and $\Omega_2 = \{x : V^a(x) \le (\eta/(1-\vartheta)\lambda_2)\}$. ϑ is a constraint satisfied $0 < \vartheta < 1$.

2.1. Fixed-wing UAV longitudinal models

In this paper, a team of n fixed-wing UAVs with a virtual leader is taken into consideration. The model of the virtual leader is considered as a first-order integral system and the models of follower UAVs is given by [24]

$$\dot{x}_i = V_i \cos\gamma_i \tag{2}$$

$$\dot{V}_i = -\frac{D_i}{m_i} + \frac{T_i \cos\alpha_i}{m_i} - g\sin\gamma_i \tag{3}$$

$$\dot{z}_i = V_i \sin\gamma_i \tag{4}$$

$$\dot{\gamma}_i = \frac{L_i - m_i g\cos\gamma_i + T_i \sin\alpha_i}{m_i V_i} \tag{5}$$

$$\dot{\alpha}_i = q_i - \frac{L_i - m_i g\cos\gamma_i + T_i \sin\alpha_i}{m_i V_i} \tag{6}$$

$$\dot{q}_i = \frac{M_i}{I_{iy}} \tag{7}$$

where x_i and z_i are the forward position and altitude position of the ith UAV in the inertial frame for $i \in \{1, 2, \cdots, n\}$, respectively. Denote the set of the positions of UAVs $p(t) = \{p_1(t), p_2(t), \ldots, p_n(t)\}$, where $p_i(t) = [x_i(t), z_i(t)]^T$ is the position of the ith UAV. V_i is the velocity, γ_i is the flight path angle, α_i is the angle of attack, and q_i is the pitch rate. m_i, g and I_{iy} are the mass of the ith UAVs, gravitational acceleration, and the moment of inertia about the pitch axis, respectively. T_i, D_i and L_i are the trust, drag and lift force, respectively. M_i is the pitch moment. The parameters and coefficient values of UAVs can be referred to [25].

Assumption 1 *([24]).* Since γ_i is quite small when UAVs are in the cruise phase, $\sin(\gamma_i) \approx \gamma_i$ is accepted in the controller design.

Based on the functional decomposition, the longitudinal dynamics of the UAVs can be divided into the position subsystem (2), (4), the velocity subsystem (3) and the flight path angle subsystem (5)–(7). To facilitate the control law design, (2)–(7) can be rewritten as

$$\begin{cases} \dot{x}_{i1} = g_{ix} x_{i2} \\ \dot{x}_{i2} = f_{i1}(x_{i2}, x_{i5}) + g_{iV} T_i \\ \dot{x}_{i3} = V_i x_{i4} \\ \dot{x}_{i4} = f_{i2}(x_{i2}, x_{i4}, x_{i5}, T_i, \delta_{ie}) + x_{i5} \\ \dot{x}_{i5} = f_{i3}(x_{i2}, x_{i4}, x_{i5}, T_i, \delta_{ie}) + x_{i6} \\ \dot{x}_{i6} = f_{i4}(x_{i2}, x_{i5}, x_{i6}, \delta_{ie}) + \delta_{ie} \end{cases} \tag{8}$$

where $f_{i1}(x_{i2}, x_{i5}) = -D_i/m_i - g\sin\gamma_i$, $f_{i2}(x_{i2}, x_{i4}, x_{i5}, T_i, \delta_{ie}) = (L_i - m_i g\cos\gamma_i + T_i \sin\alpha_i)/m_i V_i - \alpha_i$, $g_{iV} = \cos\alpha_i/m_i$, $g_{ix} = \cos\gamma_i$, $f_{i3}(x_{i2}, x_{i4}, x_{i5}, T_i, \delta_{ie}) = -(L_i - m_i g\cos\gamma_i + T_i \sin\alpha_i)/m_i V_i$, and $f_{i4}(x_{i2}, x_{i5}, x_{i6}, \delta_{ie}) = M_i/I_{iy} - \delta_{ie}$. From (8), it can be found that algebraic loops will be introduced into the control scheme if α_i and δ_{ie} are handled as the control signals. Thus, to remove the algebraic loops, the Butterworth low-pass filters (BLFs) in [44] are employed as $\alpha_{if} = B_{i\alpha}(s)\alpha_i$ and $\delta_{ief} = B_{i\delta}(s)\delta_{ie}$, where $B_{i\alpha}(s)$ and $B_{i\delta}(s)$ are the transfer function of the low-pass filters. The filter errors are defined as $\omega_{i\alpha f} = f_{i2}(V_i, \alpha_i, \gamma_i, T_i, \delta_{ie}) - f_{i2}(V_i, \alpha_{if}, \gamma_i, T_i, \delta_{ie})$ and $\omega_{i\delta f} = f_{i4}(V_i, \alpha_i, q_i, \delta_{ie}) - f_{i4}(V_i, \alpha_i, q_i, \delta_{ief})$, where $|\omega_{i\alpha f}| \le \bar{\omega}_{i\alpha f}$ and $|\omega_{i\delta f}| \le \bar{\omega}_{i\delta f}$.

2.2. Radial basis function neural network

In this paper, the RBFNN is used to deal with the unknown dynamic parameters problem in the longitudinal model of the UAV. As mentioned in [45], the ideal weight vector θ^* can be applied to express the equivalent expression of the stochastic continuous function $F(Z)$, that is

$$F(Z) = \theta^{*T}\varphi(Z) + \omega \tag{9}$$

where $\theta^* = [\theta_1, \theta_2, \ldots, \theta_l]^T \in \Re^l$ is the ideal weighting vector with l being the number of RBFNN nodes, $Z = [Z_1, Z_2, \ldots, Z_m]^T \in \Re^m$ is the input vector, and ω is the additional approximation error. $\varphi(Z) = [\varphi_1(Z), \varphi_2(Z), \ldots, \varphi_l(Z)]^T \in \Re^l$ is the Gaussian basis function vector which is given by

$$\varphi_i(Z) = \exp\left(-\frac{\|Z - C_{ei}\|_2^2}{n_i^2}\right), \quad i = 1, 2, \ldots, l \tag{10}$$

where C_{ei} and n_i represent the center and width of the ith neural cell, respectively.

2.3. Formation reconfiguration algorithm

The novel formation reconfiguration algorithm is proposed in this section, which is the basis of the collision avoidance scheme in this paper. By utilizing this formation reconfiguration algorithm, a collision avoidance area $\Omega_{ib}(t)$ as shown in Fig. 1 for each UAV will be constructed. If each UAV is limited in its collision avoidance area during the flight, there will be no collisions between UAVs. Assuming that the desired relative distance $d_{il} \in \Re^2$, between the ith desired formation position $p_{ip}(t) \in \Re^2$ and the position of virtual leader $p_l(t)$, is designed well in advance. The desired formation positions can be obtained as $p_{ip}(t) = d_{il} + p_l(t)$ for $i = 1, 2, \ldots, n$ and the set of the desired formation positions is expressed as $p_p(t) = \{p_{1p}(t), p_{2p}(t), \ldots, p_{np}(t)\}$. The task of the formation reconfigurations algorithm is choosing the desired formation position $p_{jp}(t)$ from the set $p_p(t)$ as the position command $p_{id}(t)$ for the ith UAV, which means $p_{id}(t) = p_{jp}(t)$ for $i, j = 1, 2, \ldots, n$.

To introduce the formation reconfiguration algorithm, it is necessary to define the leader-fixed reference frame (LFRF) whose origin is fixed at the position of the virtual leader and the X, Z-axis directions of the LFRF are parallel to that in the inertial frame. Define the set of desired formation positions p_p in the LFRF as $\bar{p}_p = \{\bar{p}_{1p}, \bar{p}_{2p}, \ldots, \bar{p}_{np}\} = \{d_{1l}, d_{2l}, \ldots, d_{nl}\}$ and the convex hull for $\bar{p}_p$ in the LFRF is $Co(\bar{p}_p)$. Take the set of the initial positions of UAVs in the LFRF as $\bar{p}(0) = \{\bar{p}_1(0), \bar{p}_2(0), \ldots, \bar{p}_n(0)\}$ and the convex hull for $\bar{p}(0)$ is $Co(\bar{p}(0))$. There are some reasonable assumptions about the initial position of UAVs and the desired formation positions to make them match properly.

Assumption 2. The convex hull $Co(\bar{p}_p)$ and the convex hull $Co(\bar{p}(0))$ do not overlap and the minimum x coordinate in $Co(\bar{p}_p)$ is larger than the maximum x coordinate in $Co(\bar{p}(0))$.

Remark 1. In most fixed-wing UAVs formation missions [24,25,46], the desired formation positions fixed with the virtual leader are in front of the follower UAVs at the initial time as described in Assumption 2, because the fixed-wing UAVs cannot hover or fly backward.

Assumption 3. The initial position of arbitrary UAV in the team is not on the lines that go through arbitrary two desired formation positions and the arbitrary desired formation position is not on the lines that go through arbitrary two initial positions of UAVs in the LFRF, which means that $\bar{p}_{mp} \neq \bar{p}_i(0) + \lambda\left(\bar{p}_i(0) - \bar{p}_j(0)\right)$ and $\bar{p}_m(0) \neq \bar{p}_{ip} + \bar{\lambda}\left(\bar{p}_{ip} - \bar{p}_{jp}\right)$ for $m, i, j = 1, 2, \ldots, n$ $i \neq j$, where λ and $\bar{\lambda} \in \Re$.

Remark 2. In the formation missions, Assumption 3 can be easily satisfied because of the flexibility of the initial position of follower UAVs. If there are three points collinear, it just needs to change the position of the follower UAV to make the three points non-collinear.

Under the assumptions, Algorithm 1 is proposed for properly choosing the position commands set $\bar{p}_{id}$ for the ith UAVs and it will help to avoid collisions.

Algorithm 1 The formation reconstruction algorithm for the team of UAVs

Input: $\bar{p}_{ip}$ and $\bar{p}_i(0)$ in the LFRF for $i \in \{1, 2, \ldots, n\}$.

1. Sort UAVs based on their z coordinates from small to large and index them from *1* to n. The index of the ith UAV is S_i for $i \in \{1, 2, \ldots, n\}$. Define the set of indexes
$$S = \{S_1, S_2, \ldots, S_n\}. \tag{11}$$
2. Chose the position of the ith UAV with the minimum index S_i in the set S as the starting point of a ray.
3. The ray scans clockwise from the negative side of the x-axis in the LFRF.
4. **While** $S \neq \varnothing$ **and** $\bar{p}_p \neq \varnothing$ **then**
5. **If** the first point that the ray hits is $\bar{p}_{jp}$ that belongs to $\bar{p}_p$ **then**
$$\begin{cases} S = S \backslash \{S_i\} \\ \bar{p}_p = \bar{p}_p \backslash \{\bar{p}_{jp}\} \end{cases}. \tag{12}$$
6. The ith UAV and the jth desired formation position are matched, which means $\bar{p}_{id} = \bar{p}_{jp}$ and $p_{id}(t) = p_{jp}(t)$.
7. **Return 2.**
8. **Else if** the first point that the ray hits is another UAV $\tilde{i}$ **then**
9. Change the starting point of the ray from the position of the UAV i to the position of the UAV $\tilde{i}$.
10. **Return 3.**
11. **End if.**
12. **End while**
13. **Return**
$$\begin{cases} p_d(t) = \{p_{1d}(t), p_{2d}(t), \ldots, p_{nd}(t)\} \\ \bar{p}_d = \{\bar{p}_{1d}, \bar{p}_{2d}, \ldots, \bar{p}_{nd}\} \end{cases}. \tag{13}$$

It is noticed that the condition for the line segment $\bar{p}_i(0)\bar{p}_{id}$ and another line segment $\bar{p}_j(0)\bar{p}_{jd}$ to intersect is that $\bar{p}_j(0)$ and $\bar{p}_{jd}$ are on the different sides of the straight line $\bar{p}_{id} + \lambda\bar{b}_i$ where $\bar{b}_i = \bar{p}_{id} - \bar{p}_i(0) \in \Re^2$ and $\lambda \in \Re$. However, this condition can never be satisfied under Algorithm 1 and Assumption 2, 3. Consequently, the line segments between UAVs and their position commands in the LFRF do not intersect each other. In other words, there is a minimum distance $\varepsilon_{ij} > 0$ between line segments $\bar{p}_i(0)\bar{p}_{id}$ and $\bar{p}_j(0)\bar{p}_{jd}$ for each two UAVs. The minimum of the minimum distance for the ith UAV is defined as $\bar{\varepsilon}_i = \min(\varepsilon_{ij})$ for $j \in \{1, 2, \ldots, n\} \backslash \{i\}$. Thus, as Fig. 1 shows, there will be no collisions between UAVs if the ith UAV moves in the collision avoidance region $\bar{\Omega}_{ib}$ defined in LFRF for $i \in \{1, 2, \ldots, n\}$, where

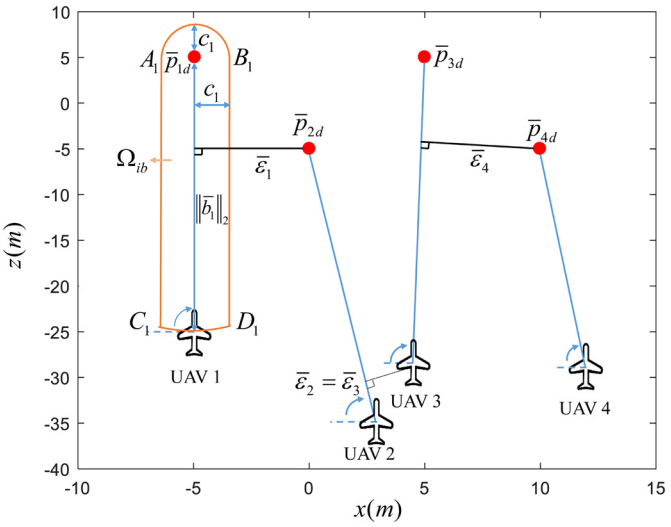

Fig. 1. The schematic diagram of the region $\Omega_{ib}(t)$.

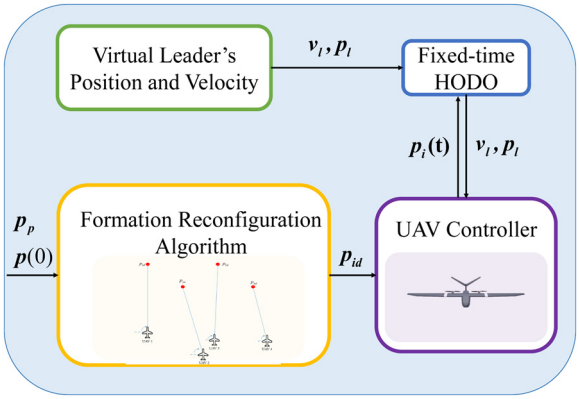

Fig. 2. The architecture of the information flow.

$0 < c_i < \bar{\varepsilon}_i/2$ is the radius of the arc A_iB_i with $\bar{p}_{id}$ as the center and $\left\|\bar{b}_i\right\|_2$ is the radius of the arc C_iD_i with $\bar{p}_{id}$ as the center. The region mapped from $\bar{\Omega}_{ib}$ to the inertial frame is denoted as $\Omega_{ib}(t)$.

3. Finite-time distributed control scheme without collision

As Fig. 2 shows, the ith follower UAV can get the information of the virtual leader by introducing the fixed-time high-order distributed observer (HODO) in [47] and confine itself in the region $\Omega_{ib}(t)$ during the flight by the distributed finite-time controller designed in this section. Designed by the backstepping method, the controller is divided into three parts, the position subsystem, the velocity subsystem, and the flight path angle subsystem. To confine the UAVs in the collision avoidance area $\Omega_{ib}(t)$, the control law for the position subsystem is very unusual, which is based on the novel Lyapunov function composed of prescribed performance and the position error term. Thus, the details of the Lyapunov function that replaces the traditional Lyapunov function are introduced in Subsection 3.1 firstly. Then, the control laws and adaptive laws considering the input saturation are proposed for three subsystems in Subsection 3.2. Finally, the stability of the UAV systems is analyzed in Subsection 3.3.

3.1. Design for the novel Lyapunov function composed of prescribed performance and the position error term

In this subsection, the novel Lyapunov function is designed by the prescribed performance and the position error term based on nonlinear mapping technology to keep the ith UAV move in $\Omega_{id}(t)$. It can be divided into two parts. One is the prescribed performance term introduced in **Step 1**, and the other one is the novel position error term introduced in **Step 2**.

Step 1. Transformation with prescribed performance

The first step to confine the ith UAV to the region $\Omega_{id}(t)$ is to confine it to the region $\Omega_{il}(t)$ defined in (15), which is the neighborhood of the line $p_{id}(t) + \lambda\bar{b}_i$ defined in the inertial frame for $\lambda \in \Re$ (see, Fig. 3(a)). To facilitate formula derivation, define that

$$\begin{cases} \bar{a}_i(t) = p_i(t) - p_{id}(t) = p_i(t) - p_l(t) - \bar{p}_{id} \\ \bar{b}_i = \bar{p}_i(0) - \bar{p}_{id} \end{cases}. \tag{14}$$

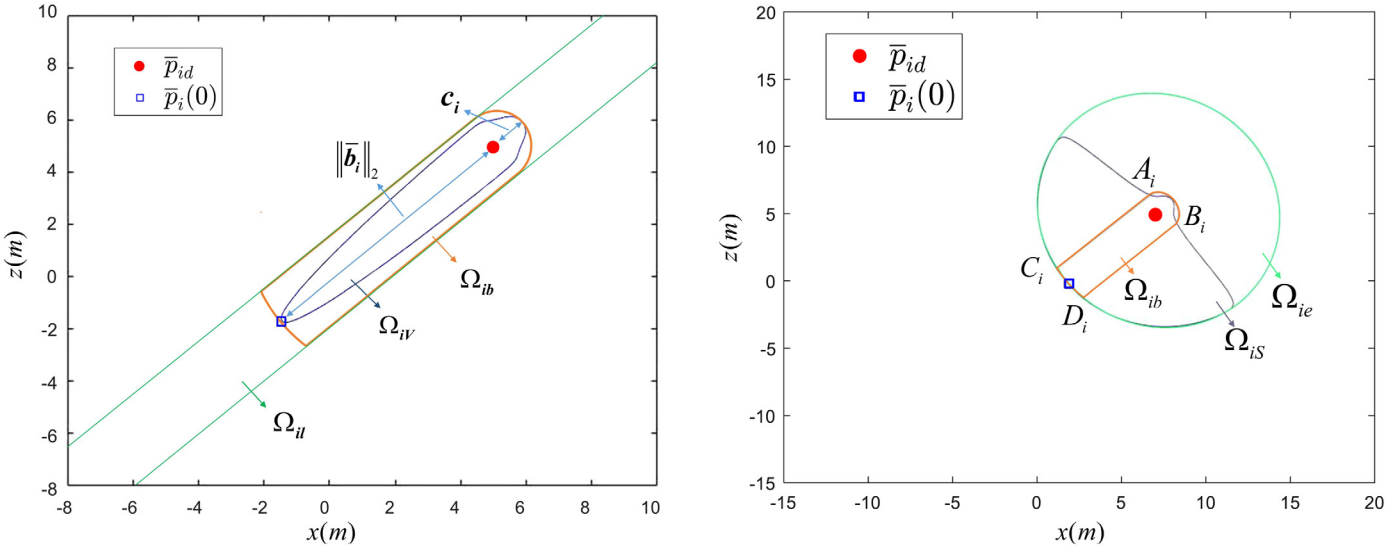

(a) The diagram of the regions $\Omega_{il}(t)$ and $\Omega_{iV}(t)$

(b) The diagram of the regions $\Omega_{iS}(t)$ and $\Omega_{ie}(t)$.

Fig. 3. The schematic diagram of the regions.

Then, $\Omega_{il}(t)$ is denoted as

$$\Omega_{il}(t) = \left\{ p_i(t) \middle| \left(\bar{a}_i[1]\bar{b}_i[2] - \bar{a}_i[2]\bar{b}_i[1] \right) / \left\| \bar{b}_i \right\|_2 \right| \le c_i \right\}. \tag{15}$$

From (15), it can be seen that the distance between any position in Ω_{il} and the line $p_{id}(t) + \lambda \bar{b}_i$ is less than c_i. Thus, the ith UAV is confined to Ω_{il} iff

$$-c_i \le l_i = \left(\bar{a}_i[1]\bar{b}_i[2] - \bar{a}_i[2]\bar{b}_i[1] \right) / \left\| \bar{b}_i \right\|_2 \le c_i \tag{16}$$

where $|l_i|$ is the distance from the position of ith UAV to the line $p_{id}(t) + \lambda \bar{b}_i$. To make l_i satisfy (16), the performance function $\varpi_i(t)$ is introduced. To better fit the prescribed performance control, and the condition (16) can be stricter as $-c_i\varpi_i(t) \le l_i \le c_i\varpi_i(t)$, where $\varpi_i(t)$ is a strictly positive decreasing smooth function. It is chosen that $\varpi_i(t) = (\varpi_{i0} - \varpi_{i\infty})e^{-\kappa_i t} + \varpi_{i\infty}$, where $\varpi_{i0} \in \Re$ and $\varpi_{i\infty} \in \Re$ satisfy $1 > \varpi_{i0} > \varpi_{i\infty} > 0$ and $\kappa_i > 0$ is the decreasing rate. For simplifying the derivation, the inequality can be transformed into an equality form as $l_i(t) = \varpi_i(t) f_{tran}(\varepsilon_i(t))$, where $\varepsilon_i(t)$ is the transformed error for the ith UAV. The function $f_{tran}(\varepsilon)$ has the following property:

1) It is a smooth and monotonic increasing function
2) $f_{tran}(0) = 0$
3) $\lim_{\varepsilon \to +\infty} f_{tran}(\varepsilon) = 1$ and $\lim_{\varepsilon \to -\infty} f_{tran}(\varepsilon) = -1$.

According to the requirements of predictive performance control, the initial state of l_i must satisfy $-c_i \le l_i(0) \le c_i$. However, due to the ingenuity of the design of Algorithm 1, $l_i(0) = 0$, which means that c_i can take arbitrarily small positive numbers.

In this paper, $f_{tran}(\varepsilon)$ is chosen as $f_{tran}(\varepsilon) = \left(e^{\varepsilon} - e^{-\varepsilon}\right) / \left(e^{\varepsilon} + e^{-\varepsilon}\right)$. Then, the transformed errors can be expressed as $\varepsilon_i = f_{tran}^{-1}(l_i/\varpi_i) = (1/2)\ln\left((1 + l_i/\varpi_i)/(1 - l_i/\varpi_i)\right)$. The time derivative of ε_i is

$$\begin{aligned} \dot{\varepsilon}_i &= \frac{\partial f_{tran}^{-1}(l_i/\varpi_i)}{\partial (l_i/\varpi_i)} \frac{d(l_i/\varpi_i)}{dt} \\ &= \left(\frac{1}{(1 + l_i/\varpi_i)(1 - l_i/\varpi_i)} \right) \left(\frac{\dot{l}_i\varpi_i - l_i\dot{\varpi}_i}{\varpi_i^2} \right) \\ &= \rho_i \left(\bar{b}_i' (\dot{p}_i - \dot{p}_{id}) - \frac{l_i\dot{\varpi}_i}{\varpi_i} \right) \end{aligned} \tag{17}$$

where $\rho_i = (1/2)\left(1/(\varpi_i + l_i) + 1/(\varpi_i - l_i)\right)$ and $\bar{b}_i' = \left[\bar{b}_i[2] / \left\| \bar{b}_i \right\|_2, -\bar{b}_i[1] / \left\| \bar{b}_i \right\|_2 \right]$.

If the transformed errors $\varepsilon_i(t)$ for $i \in \{1, 2, \ldots, n\}$ are confined to a neighborhood of the origin, it means that the ith UAV is contained in $\Omega_{il}(t)$. Furthermore, to achieve collision avoidance, the movement area of the ith UAV needs to be further reduced in $\Omega_{ib}(t)$. It needs to ensure that the ith UAV is contained in the region between the arc A_iB_i and C_iD_i as shown in Fig. 3(b). To achieve that goal, the position error term is proposed in **Step 2**.

Step 2. Design of the position error term

To keep the ith UAV moves between the arc A_iB_i and C_iD_i and achieve $p_i(t) \to p_{id}(t)$ in the meantime, a novel position error function is designed. Recalling the position model (1), (3), the position subsystem of the ith UAV can be rewritten as

$$\dot{p}_i = g_{ip} p_{i2} \tag{18}$$

where $p_i = [x_{i1}, x_{i3}]^T$, $g_{ip} = diag\{g_{iV}, V_i\}$ and $p_{i2} = [x_{i2}, x_{i4}]^T$. The novel error S_{ie} is designed as

$$S_{ie} = f_{ie}(l_i^1) e_{ip} \tag{19}$$

where $e_{ip} = p_i - p_{id}$ and $l_i^1 = \left(\bar{a}_i[1]\bar{b}_i^1[2] - \bar{a}_i[2]\bar{b}_i^1[1]\right) / \left\|\bar{b}_i^1\right\|_2$ for $\bar{b}_i^1 = \left[\bar{b}_i[2], -\bar{b}_i[1]\right]^T$. $|l_i^1|$ means the distance between $p_i(t)$ and the line $p_{id}(t) + \lambda\bar{b}_i^1$ which is perpendicular to the line $p_{id}(t) + \lambda\bar{b}_i$ in the inertial frame. The function $f_{ie}(l_i^1)$ is expressed as

$$f_{ie}\left(l_i^1\right) = \tau_i \tanh\left(l_i^1\right) + m_{li} \tag{20}$$

where $m_{li} = 1/1 - \sigma_i > 1$, $\tau_i = m_{li}\sigma_i = m_{li} - 1 > 0$ and $\sigma_i = \left(c_i - \left\|\bar{b}_i\right\|_2\right) / \left(\left\|\bar{b}_i\right\|_2 \tanh\left(-\left\|\bar{b}_i\right\|_2\right) - c_i \tanh(c_i)\right) \in (0, 1)$. It is noticed that $f_{ie}\left(l_i^1\right)$ satisfies the following properties, which will be used in stability analysis.

1) It is a smooth and monotonic increasing function
2) $1 < f_{ie}\left(l_i^1\right) < 2m_{li} - 1$
3) $f_{ie}\left(-\left\|\bar{b}_i\right\|_2\right) / f_{ie}(c_i) = c_i / \left\|\bar{b}_i\right\|_2$.

Due to $f_{ie}\left(l_i^1\right) > 0$, $S_{ie}^T S_{ie}$ is a positive definite function of e_{ip}. Take the time derivative of (19)

$$\begin{aligned} \dot{S}_{ie} &= \frac{\partial f_{ie}\left(l_i^1\right)}{\partial l_i^1}\frac{dl_i^1}{dt} e_{ip} + f_{ie}\left(l_i^1\right)\frac{de_{ip}}{dt} \\ &= \frac{\tau_i}{\cosh\left(l_i^1\right)^2}\bar{b}_i^{1'}(\dot{p}_i - \dot{p}_{id}) e_{ip} + f_{ie}\left(l_i^1\right)(\dot{p}_i - \dot{p}_{id}) \end{aligned} \tag{21}$$

where $\bar{b}_i^{1'} = \left[\bar{b}_i^1[2] / \left\|\bar{b}_i^1\right\|_2, -\bar{b}_i^1[1] / \left\|\bar{b}_i^1\right\|_2\right]$.

It needs to be noticed that the reason why we chose the novel error $V_{S_{ie}} = S_{ie}^T S_{ie}/2$ rather than the error $V_{ie} = e_{ip}^T e_{ip}/2$ to design the Lyapunov function is it will be utilized to control the ith UAV to move in the region $\Omega_{iS}(t) = \left\{p_i(t) | V_{S_{ie}}(p_i(t)) \le V_{S_{ie}}(p_i(0))\right\}$ rather than the region $\Omega_{ie}(t) = \{p_i(t) | V_{ie}(p_i(t)) \le V_{ie}(p_i(0))\}$ (see Fig. 3(b)). By utilizing the scale factor $f_{ie}(l_i^1)$, the position error S_{ie} will ultimately help the ith UAV to move between the arc A_iB_i and C_iD_i which are the boundary of $\Omega_{ib}(t)$.

Step 3. The novel Lyapunov function composed of the prescribed performance and the position error term

According to the above introduction, combining the prescribed performance term and the position error term, the general Lyapunov function is

$$V_{i1} = V_{S_{ie}} + \frac{1}{2}\varepsilon_i^2 \tag{22}$$

Remark 3. As shown in Fig. 3(a), if $V_{i1}(t) \le V_{i1}(0)$ for $t > 0$, the ith UAV will be confined to $\Omega_{iV}(t) = \{p_i(t) | V_{i1}(p_i(t)) \le V_{i1}(p_i(0))\} \subseteq \Omega_{ib}(t)$, which can enable no collisions between UAVs during the flight. The proof of $V_{i1}(t) \le V_{i1}(0)$ for $t > 0$ is shown in subsection 3.3.

3.2. Finite-time backstepping controller design for the UAVs

In this paper, the controller design is divided into three parts as the position subsystem, the velocity subsystem, and the flight path angle subsystem. Recalling the UAV model (8), the position subsystem is composed of states x_{i1} and x_{i3}, which can control the UAVs form the formation and avoid collisions by utilizing the method mentioned in Section 3.1. The velocity subsystem composed of state x_{i2} and the flight path angle subsystem composed of state x_{i4}, x_{i5} and x_{i6} are designed to track the virtual velocity and flight path angle command signals provided by the position subsystem, respectively. Due to the different orders, the control laws for the velocity subsystem and flight path angle subsystem are designed separately.

3.2.1. Finite-time controller design for the position subsystem

As mentioned in Section 3.1, the virtual control signal $\bar{p}_{i2}$ for the position subsystem is based on the novel Lyapunov function (22), which is designed as

$$\bar{p}_{i2} = g_{i1}^{-1}\left(\dot{p}_{id} - \mu_i^{-1}\left(k_{i11}S_{ie} + k_{i12}sig^{r_i}(S_{ie}) + k_{i15}sig^3(S_{ie})\right) - \rho_i^{-1}\bar{b}_i^{\prime T}\left(k_{i13}\varepsilon_i + k_{i14}sig^{r_i}(\varepsilon_i) - \rho_i\frac{l_i\dot{\varpi}_i}{\varpi_i}\right)\right) \tag{23}$$

where $\mu_i = \left(\tau_i\bar{b}_i^{1'}e_{ip} / \cosh\left(l_i^1\right)^2 + f_{ie}\left(l_i^1\right)\right)$. k_{i11}, k_{i12}, k_{i13}, k_{i14} and k_{i15} are the positive control parameters. $r_i = k_p/k_q$, where k_p and k_q are positive odd numbers satisfy $k_q < k_p < 2k_q$.

Based on the backstepping method, the designed virtual control input $\bar{p}_{i2}$ can be regarded as the virtual command signal $\bar{V}_i = \bar{x}_{i2} = \bar{p}_{i2}[1]$ for the velocity subsystem and the command signal $\bar{\gamma}_i = \bar{x}_{i4} = \bar{p}_{i2}[2]$ for the flight path angle subsystem (see, Fig. 4), respectively.

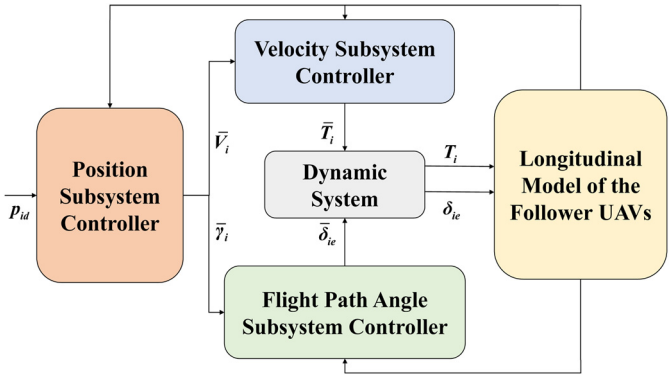

Fig. 4. The architecture of the controller.

3.2.2. Finite-time controller design for the velocity subsystem

In this section, considering the asymmetric input saturation and parameter unknown problem, the finite-time controller based on the backstepping method for the velocity subsystem is proposed to achieve $V_i \to \bar{V}_i$ in a finite time. Define the errors of the velocity subsystem of the ith UAV

$$\begin{cases} e_{i2} = x_{i2} - \bar{x}_{i2} \\ e_{iT} = T_i - \bar{T}_i - \zeta_{i1} \end{cases} \tag{24}$$

where $\bar{T}_i$ is a virtual control signal designed by the backstepping method latter and ζ_{i1} is an auxiliary signal constructed to compensate for the input saturation, e_{i2} is the tracking error of the velocity. From (24), the velocity subsystem is changed from the first-order system to the second-order system to deal with the input saturation issue.

STEP 1: In order to avoid the differential explosion problem, $\dot{\bar{x}}_{i2}$ can be obtained by employing the differentiator in [47], which can be expressed as $\dot{\bar{x}}_{i2} = \dot{\bar{x}}_{i2o} + \omega_{iV}$, where $\dot{\bar{x}}_{i2o}$ is the estimate of $\dot{\bar{x}}_{i2}$ and ω_{iV} is the estimate error bounded by $|\omega_{iV}| \le \bar{\omega}_{iV}$. Besides, to deal with the unknown parameters by RBFNN, the formula $f_{i1}(x_{i2}, x_{i5}) = \theta_{i1}^{*T}\varphi_{i1}(x_{i2}, x_{i5}) + \omega_{i1}$ can be obtained, where φ_{i1} is the basis function vector of RBFNN. Then, the desired control input signal and adaptive laws are designed as

$$\begin{cases} \bar{T}_i = g_{iV}^{-1}\left(-k_{i21}e_{i2} - k_{i22}sig^{r_i}(e_{i2}) - \dfrac{e_{i2}\hat{\chi}_{i1}\varphi_{i1}^T\varphi_{i1}}{2\xi_{2i}^2} - \dfrac{e_{i2}\hat{\chi}_{i2}}{2\xi_{3i}^2} + \dot{\bar{x}}_{i2o}\right) - \zeta_{i1} \\ \dot{\hat{\chi}}_{i1} = g_{i21}\left(\dfrac{e_{i2}^2\varphi_{i1}^T\varphi_{i1}}{2\xi_{2i}^2} - h_{i21}\hat{\chi}_{i1}\right) \\ \dot{\hat{\chi}}_{i2} = g_{i22}\left(\dfrac{e_{i2}^2}{2\xi_{3i}^2} - h_{i22}\hat{\chi}_{i2}\right) \end{cases} \tag{25}$$

where k_{i21}, k_{i22}, ξ_{2i}, ξ_{3i}, g_{i21}, h_{i21}, g_{i22} and h_{i22} are the positive parameters. $\hat{\chi}_{i1}$ and $\hat{\chi}_{i2}$ are the adaptive signal of $\chi_{i1} = \theta_{i1}^{*T}\theta_{i1}^{*}$ and $\chi_{i2} = (\bar{\omega}_{i1} + \bar{\omega}_{iV})^2$, respectively. It is noticed that the minimum parameter learning of RBFNN (MPLNN) is utilized in the controller design, which greatly reduces the computation.

STEP 2: Because the input signal, in engineering systems, is often encountered by asymmetric saturation. Therefore, inspired by [27], the following dynamic system is tactfully constructed to generate the control input T_i. Assume that

$$T_i = \frac{T_{\max}}{2} + \frac{T_{\max}}{2}\tanh\left(\frac{2T_{if}}{T_{\max}}\right) \tag{26}$$

where $T_{\max}$ is the maximum input signal and $T_{if} \in \Re$ is an auxiliary intermediate signal that is yet to be designed. Taking the time derivative of T_i, it can be got that $\dot{T}_i = \cosh^{-2}(2T_{if}/T_{\max})\dot{T}_{if}$. To compensate for the adverse effect arising from input saturation, the auxiliary system is introduced as $\dot{\zeta}_{i1} = -k_{i23}\zeta_{i1} + \Delta T_i$, where $\zeta_{i1} \in \Re$ is the auxiliary state signal, k_{i23} is a positive design parameter and $\Delta T_i = \dot{T}_i - \bar{T}_{if}$ is the deviation between the signals $\bar{T}_{if}$ and $\dot{T}_i$, which are designed as

$$\begin{cases} \bar{T}_{if} = -k_{i24}e_{iT} - g_{iV}^{-1}e_{i2} + \dot{\bar{T}}_{io} - k_{i23}\zeta_{i1} - \dfrac{e_{iT}\hat{\chi}_{i3}}{2\xi_{i4}^2} \\ \dot{T}_{if} = k_{i25}\bar{T}_{if} \end{cases} \tag{27}$$

where k_{i24}, k_{i25} and ξ_{4i} are positive design parameters and $\dot{\bar{T}}_{io}$ is the estimate of the time derivative of $\dot{\bar{T}}_i$ by using the differentiator in [47], which satisfies that $\dot{\bar{T}}_i = \dot{\bar{T}}_{io} + \omega_{iT}$ and $|\omega_{iT}| \le \bar{\omega}_{iT}$. $\hat{\chi}_{i3}$, the adaptive signal of $\chi_{i3} = \bar{\omega}_{iT}^2$, satisfies that

$$\dot{\hat{\chi}}_{i3} = g_{i23}\left(\frac{e_{iT}^2}{2\xi_{4i}^2} - h_{i23}\hat{\chi}_{i3}\right) \tag{28}$$

where g_{i23} and h_{i23} are positive design parameters.

Remark 4. According to the design approach of the dynamic system, the control input T_i is limited to $(0, T_{\max})$ for all time. Compared with the method that directly utilizing the auxiliary system like [24–26,28], the dynamic system (24)–(26) is continuous and can effect to enforce the compensation function when input saturation reappears. Compared with the dynamic system constructed to compensate for the input saturation in [27], the dynamic system (24)–(26) does not have the time-varying limit and can compensate for both symmetric input saturation and asymmetric input saturation problems.

3.2.3. Finite-time controller design for flight path angle subsystem

In this subsection, the finite-time controller considering the symmetric input saturation and unknown parameter problem, for the flight path angle subsystem, is proposed to achieve $\gamma_i \to \bar{\gamma}_i$ in a finite time.

Define the errors of the flight path angle subsystem of the ith UAV as

$$e_{ij} = x_{ij} - \bar{x}_{ij} \quad \text{for } j \in \{4, 5, 6\} \tag{29}$$

$$e_{i\delta} = \delta_{ie} - \bar{\delta}_{ie} - \zeta_{i2} \tag{30}$$

where e_{i4}, e_{i5}, e_{i6} and $e_{i\delta}$ are the tracking error of flight path angle, angle of attack, pitch rate and elevator deflection angle, respectively. $\bar{x}_{i4}$, $\bar{x}_{i5}$, $\bar{x}_{i6}$ and $\bar{\delta}_{ie}$ are the virtual control signal of flight path angle, angle of attack, pitch rate and elevator deflection angle designed by backstepping method. ζ_{i2} is an auxiliary signal constructed to compensate for the input saturation.

STEP 1: In order to avoid the differential explosion problem, $\dot{\bar{x}}_{i4}$, $\dot{\bar{x}}_{i5}$ and $\dot{\bar{x}}_{i6}$ can be obtained by employing the differentiator in [47], which satisfy $\dot{\bar{x}}_{i4o} = \dot{\bar{x}}_{i4} - \omega_{i\gamma}$, $\dot{\bar{x}}_{i5o} = \dot{\bar{x}}_{i5} - \omega_{i\alpha}$ and $\dot{\bar{x}}_{i6o} = \dot{\bar{x}}_{i6} - \omega_{iq}$ where $\dot{\bar{x}}_{i4o}$, $\dot{\bar{x}}_{i5o}$ and $\dot{\bar{x}}_{i6o}$ are the estimate values. $\omega_{i\gamma}$, $\omega_{i\alpha}$ and ω_{iq} are the estimate errors bounded by $|\omega_{i\gamma}| \le \bar{\omega}_{i\gamma}$, $|\omega_{i\alpha}| \le \bar{\omega}_{i\alpha}$ and $|\omega_{iq}| \le \bar{\omega}_{iq}$. Besides, to deal with the unknown parameters by RBFNN, the formula $f_{ij}(x_{i2}, x_{i4}, x_{i5}, T_i, \delta_{ie}) = \theta_{ij}^{*T}\varphi_{ij}(x_{i2}, x_{i4}, x_{i5}, T_i, \delta_{ie}) + \omega_{ij}$ for $j \in \{2, 3, 4\}$ can be obtained, where φ_{i2}, φ_{i3} and φ_{i4} are the basis function vectors of RBFNN. Then, the designed control input of flight path angle subsystem and adaptive laws are designed as

$$\begin{cases} \bar{x}_{i5} = -k_{i31}e_{i4} - k_{i32}sig^{r_i}(e_{i4}) + \dot{\bar{x}}_{i4o} - \dfrac{e_{i4}\hat{\chi}_{i4}\varphi_{i2}^T\varphi_{i2}}{2\xi_{5i}^2} - \dfrac{e_{i4}\hat{\chi}_{i5}}{2\xi_{6i}^2} \\ \bar{x}_{i6} = -k_{i33}e_{i5} - k_{i34}sig^{r_i}(e_{i5}) + \dot{\bar{x}}_{i5o} - e_{i4} - \dfrac{e_{i5}\hat{\chi}_{i6}\varphi_{i3}^T\varphi_{i3}}{2\xi_{7i}^2} - \dfrac{e_{i5}\hat{\chi}_{i7}}{2\xi_{8i}^2} \\ \bar{\delta}_{ie} = -k_{i35}e_{i6} - k_{i36}sig^{r_i}(e_{i6}) + \dot{\bar{x}}_{i6o} - e_{i5} - \dfrac{e_{i6}\hat{\chi}_{i8}\varphi_{i4}^T\varphi_{i4}}{2\xi_{9i}^2} - \dfrac{e_{i6}\hat{\chi}_{i9}}{2\xi_{10i}^2} - \zeta_{i2} \end{cases} \tag{31}$$

$$\begin{cases} \dot{\hat{\chi}}_{i4} = g_{i31}\left(\dfrac{e_{i4}^2\varphi_{i2}^T\varphi_{i2}}{2\xi_{5i}^2} - h_{i31}\hat{\chi}_{i4}\right) \\ \dot{\hat{\chi}}_{i6} = g_{i33}\left(\dfrac{e_{i6}^2\varphi_{i3}^T\varphi_{i3}}{2\xi_{7i}^2} - h_{i33}\hat{\chi}_{i6}\right) \\ \dot{\hat{\chi}}_{i8} = g_{i35}\left(\dfrac{e_{i8}^2\varphi_{i4}^T\varphi_{i4}}{2\xi_{9i}^2} - h_{i35}\hat{\chi}_{i8}\right) \end{cases} \tag{32}$$

$$\begin{cases} \dot{\hat{\chi}}_{i5} = g_{i32}\left(\dfrac{e_{i4}^2}{2\xi_{6i}^2} - h_{i32}\hat{\chi}_{i5}\right) \\ \dot{\hat{\chi}}_{i7} = g_{i34}\left(\dfrac{e_{i6}^2}{2\xi_{8i}^2} - h_{i34}\hat{\chi}_{i7}\right) \\ \dot{\hat{\chi}}_{i9} = g_{i36}\left(\dfrac{e_{i8}^2}{2\xi_{10i}^2} - h_{i36}\hat{\chi}_{i9}\right) \end{cases} \tag{33}$$

where k_{i3l}, g_{i3l}, h_{i3l} for $l \in \{1, 2, \ldots, 6\}$ and ξ_{in} for $n \in \{5, 6, \ldots, 10\}$ are the positive parameters. $\hat{\chi}_{ip}$ for $p \in \{4, 5, \ldots, 9\}$ are the adaptive signals of $\chi_{i4} = \theta_{i2}^{*T}\theta_{i2}^*$, $\chi_{i5} = (\bar{\omega}_{i2} + \bar{\omega}_{i\alpha f} + \bar{\omega}_{i\gamma})^2$, $\chi_{i6} = \theta_{i3}^{*T}\theta_{i3}^*$, $\chi_{i7} = (\omega_{i3} + \omega_{i\alpha})^2$, $\chi_{i8} = \theta_{i4}^{*T}\theta_{i4}^*$ and $\chi_{i9} = (\bar{\omega}_{i4} + \bar{\omega}_{i\delta f} + \bar{\omega}_{iq})^2$, respectively.

STEP 2: The input signal, in the elevator systems, is often encountered by symmetric saturation. Therefore, the following dynamic system is tactfully constructed to generate the control input δ_{ie}. Assume that

$$\delta_{ie} = \delta_{\max}\tanh\left(\frac{\delta_{ief}}{\delta_{\max}}\right) \tag{34}$$

where $\delta_{\max}$ is the maximum input signal and δ_{ief} is an auxiliary intermediate signal that is yet to be designed. Taking the time derivative of δ_{ie}, it can be got that $\dot{\delta}_{ie} = \cosh^{-2}(\delta_{ief}/\delta_{\max})\dot{\delta}_{ief}$. To compensate for the adverse effect arising from input saturation, we introduce the following auxiliary system. $\dot{\zeta}_{i2} = -k_{i37}\zeta_{i2} + \Delta\delta_{ie}$, where $\zeta_{i2} \in \Re$ is the auxiliary state signal, k_{i37} is a positive design parameter, and $\Delta\delta_{ie} = \dot{\delta}_{ie} - \bar{\delta}_{ief}$ is the deviation between the signals $\bar{\delta}_{ief}$ and $\dot{\delta}_{ie}$, which are designed as

$$\begin{cases} \bar{\delta}_{ief} = -k_{i38}e_{i\delta} - e_{i6} + \dot{\bar{\delta}}_{ieo} - k_{i37}\zeta_{i2} - \dfrac{e_{i\delta}\hat{\chi}_{i10}}{2\xi_{i11}^2} \\ \dot{\delta}_{ief} = k_{i39}\bar{\delta}_{ief} \end{cases} \tag{35}$$

where k_{i38}, k_{i39} and ξ_{11i} are positive design parameters and $\dot{\bar{\delta}}_{ieo}$ is the estimate of the time derivative of $\dot{\bar{\delta}}_{ie}$ by using the differentiator shown in [47], which satisfies that $\dot{\bar{\delta}}_{ie} = \dot{\bar{\delta}}_{ieo} + \omega_{i\delta}$ and $|\omega_{i\delta}| \le \bar{\omega}_{i\delta}$. $\hat{\chi}_{i10}$, the adaptive signal of $\chi_{i10} = \bar{\omega}_{i\delta}^2$, satisfies that

$$\dot{\hat{\chi}}_{i10} = g_{i37}\left(\frac{e_{i\delta}^2}{2\xi_{11i}^2} - h_{i37}\hat{\chi}_{i10}\right) \tag{36}$$

where g_{i37} and h_{i37} are positive design parameters. According to the design approach of the dynamic system, the control input δ_{ie} is limited to $(-\delta_{\max}, \delta_{\max})$ for all time.

Theorem 1. *For the team of UAVs as described in (8), by utilizing Algorithm 1 and the control laws (23), (25)–(28) and (31)–(36) designed in section 3.2, it comes to the following points:*

1. *the error states will converge to a small neighborhood of the origin and the formation will be formed in a finite time;*
2. *the ith UAV is contained in a designated area Ω_{ib} during the flight such that the team is with global collision avoidance.*

The proof of Theorem 1 is shown in section 3.3.

3.3. Stability analysis

The finite time convergence of the novel position error S_{ie} means the ith UAV will converge to the desired position in finite time. The Lyapunov function $V_{i1}(t)$ satisfied $V_{i1}(t) \le V_{i1}(0)$ for $t > 0$ means the ith UAV moves in the collision avoidance area $\Omega_{ib}(t)$ during the flight, which achieves the global collision avoidance. Thus, Theorem 1 has been proved when the above two conditions are achieved. In this subsection, the finite-time convergence of the control law is proved by the Lyapunov stability, and the proof of $V_{i1}(t) \le V_{i1}(0)$ for $t > 0$ is presented.

STEP 1: The stability analysis of the position subsystem

First of all, recalling (17) and (21), one can take the time derivative of the Lyapunov function of the position subsystem introduced in (22)

$$\begin{aligned} \dot{V}_{i1} &= S_{ie}^T\dot{S}_{ie} + \varepsilon_i\dot{\varepsilon}_i \\ &= S_{ie}^T\left(\frac{\tau_i}{\cosh\left(l_i^1\right)^2}e_{ip}\bar{b}_i^{1\prime} + f_{ie}\left(l_i^1\right)\right)(\dot{p}_i - \dot{p}_{id}) + \varepsilon_i\left(\rho_i\bar{b}_i'(\dot{p}_i - \dot{p}_{id}) - \rho_i\frac{l_i\dot{\varpi}_i}{\varpi_i}\right). \\ &= S_{ie}^T\mu_i(\dot{p}_i - \dot{p}_{id}) + \varepsilon_i\left(\rho_i\bar{b}_i'(\dot{p}_i - \dot{p}_{id}) - \rho_i\frac{l_i\dot{\varpi}_i}{\varpi_i}\right) \end{aligned} \tag{37}$$

Substitute the virtual control law (23) into (37)

$$\begin{aligned} \dot{V}_{i1} &= S_{ie}^T\mu_i\left(g_{ip}(\tilde{p}_{i2} + \bar{p}_{i2}) - \dot{p}_{id}\right) + \varepsilon_i\left(\rho_i\bar{b}_i'\left(g_{ip}(\tilde{p}_{i2} + \bar{p}_{i2}) - \dot{p}_{id}\right) - \rho_i\frac{l_i\dot{\varpi}_i}{\varpi_i}\right) \\ &\le -k_{i11}S_{ie}^TS_{ie} - k_{i12}S_{ie}^Tsig^{r_i}(S_{ie}) - k_{i15}\left\|S_{ie}^TS_{ie}\right\|_2^2 - k_{i13}\varepsilon_i^2 - k_{i14}\varepsilon_isig^{r_i}(\varepsilon_i) + \left(S_{ie}^T\mu_i + \varepsilon_i\bar{b}_i'\right)g_{ip}\tilde{p}_{i2} \end{aligned} \tag{38}$$

where $\tilde{p}_{i2} = p_{i2} - \bar{p}_{i2}$. By utilizing Young's inequality, one can obtain

$$\begin{aligned} \left(S_{ie}^T\mu_i + \varepsilon_i\bar{b}_i'\right)g_{ip}\tilde{p}_{i2} &\le \frac{\left\|S_{ie}^T\mu_i + \varepsilon_i\bar{b}_i'\right\|_2^2}{2\xi_{1i}^2} + \frac{\xi_{1i}^2\left\|g_{ip}\tilde{p}_{i2}\right\|_2^2}{2} \\ &\le \frac{3}{2\xi_{1i}^2}\left(\left\|\frac{\tau_i}{f_{ie}\left(l_i^1\right)\cosh\left(l_i^1\right)^2}S_{ie}^TS_{ie}\bar{b}_i^{1\prime}\right\|_2^2 + f_{ie}^2\left(l_i^1\right)\left\|S_{ie}^T\right\|_2^2 + \|\varepsilon_i\|_2^2\right) + \frac{\xi_{1i}^2\left\|g_{ip}\tilde{p}_{i2}\right\|_2^2}{2} \end{aligned} \tag{39}$$

where ξ_{1i} is an arbitrarily small positive constant. Noting the equality $\left\|\bar{b}_i'\right\|_2^2 = \left\|\bar{b}_i^{1\prime}\right\|_2^2 = 1$ and the compatibility of norms, (39) can be further obtained as

$$\left(S_{ie}^T\mu_i + \varepsilon_i\bar{b}_i'\right)g_{ip}\tilde{p}_{i2} \le \frac{3}{2\xi_{1i}^2}\left(\left(\frac{\tau_i}{\cosh\left(l_i^1\right)^2}\right)^2\left\|S_{ie}^TS_{ie}\right\|_2^2 + (2\tau_i + 1)^2\|S_{ie}\|_2^2 + \varepsilon_i^2\right) + \frac{\xi_{1i}^2\left\|g_{ip}\tilde{p}_{i2}\right\|_2^2}{2}. \tag{40}$$

Take (40) into (38), it can be got that

$$\begin{aligned}\dot{V}_{i1} \le &-\left(k_{i11}-\frac{3(2\tau_i+1)^2}{2\xi_{1i}^2}\right)S_{ie}^T S_{ie}-k_{i12}S_{ie}^T sig^{r_i}(S_{ie})-\left(k_{i13}-\frac{3}{2\xi_{1i}^2}\right)\varepsilon_i^2-k_{i14}sig^{r_i+1}(\varepsilon_i)\\ &-\left(k_{i15}-\frac{3}{2\xi_{1i}^2}\left(\frac{\tau_i}{\cosh\left(l_i^1\right)^2}\right)^2\right)\left\|S_{ie}^T S_{ie}\right\|_2^2+\frac{\xi_{1i}^2\left\|\tilde{p}_{i2}[1]\right\|_2^2}{2}+\frac{\xi_{1i}^2\widehat{V}_i^2\left\|\tilde{p}_{i2}[2]\right\|_2^2}{2}\end{aligned} \tag{41}$$

where $\widehat{V}_i$ is the maximum of V_i and only used for the stability analysis. $\tilde{p}_{i2}[1]=e_{i2}$ and $\tilde{p}_{i2}[2]=e_{i4}$. Thus, by designing $k_{i15}>3\tau_i^2/\left(2\xi_{1i}^2\cosh\left(l_i^1\right)^4\right)$, it can be seen that

$$\dot{V}_{i1} \le -\left(k_{i11}-\frac{3(2\tau_i+1)^2}{2\xi_{1i}^2}\right)S_{ie}^T S_{ie}-k_{i12}S_{ie}^T sig^{r_i}(S_{ie})-\left(k_{i13}-\frac{3}{2\xi_{1i}^2}\right)\varepsilon_i^2-k_{i14}sig^{r_i+1}(\varepsilon_i)+\frac{\xi_{1i}^2\left\|\tilde{p}_{i2}[1]\right\|_2^2}{2}+\frac{\xi_{1i}^2\widehat{V}_i^2\left\|\tilde{p}_{i2}[2]\right\|_2^2}{2}. \tag{42}$$

STEP 2: The stability analysis of the velocity subsystem

Secondly, choose the Lyapunov functions for the velocity subsystem as

$$V_{i2}=\frac{1}{2}e_{i2}^2+\frac{1}{2g_{i21}}\tilde{\chi}_{i1}^2+\frac{1}{2g_{i22}}\tilde{\chi}_{i2}^2 \tag{43}$$

$$V_{i3}=\frac{1}{2}e_{iT}^2+\frac{1}{2g_{i23}}\tilde{\chi}_{i3}^2 \tag{44}$$

where $\tilde{\chi}_{i1}=\chi_{i1}-\hat{\chi}_{i1}$, $\tilde{\chi}_{i2}=\chi_{i2}-\hat{\chi}_{i2}$ and $\tilde{\chi}_{i3}=\chi_{i3}-\hat{\chi}_{i3}$ are the estimation errors. The time derivative of V_{i2} is

$$\dot{V}_{i2}=e_{i2}\left(f_{i1}+g_{iV}T_i-\dot{\bar{x}}_{i2}\right)-\frac{\tilde{\chi}_{i1}\dot{\hat{\chi}}_{i1}}{g_{i21}}-\frac{\tilde{\chi}_{i2}\dot{\hat{\chi}}_{i2}}{g_{i22}}. \tag{45}$$

Consider f_{i1} is estimated by the RBFNN, and (45) can be rewritten as

$$\begin{aligned}\dot{V}_{i2}&=e_{i2}\left(\theta_{i1}^{*T}\varphi_{i1}+\omega_{i1}+g_{iV}T_i-\dot{\bar{x}}_{i2}\right)-\frac{\tilde{\chi}_{i1}\dot{\hat{\chi}}_{i1}}{g_{i21}}-\frac{\tilde{\chi}_{i2}\dot{\hat{\chi}}_{i2}}{g_{i22}}\\ &=e_{i2}\left(\theta_{i1}^{*T}\varphi_{i1}+\omega_{i1}+g_{iV}(e_{iT}+\bar{T}_i+\zeta_{i1})-\dot{\bar{x}}_{i2}\right)-\frac{\tilde{\chi}_{i1}\dot{\hat{\chi}}_{i1}}{g_{i21}}-\frac{\tilde{\chi}_{i2}\dot{\hat{\chi}}_{i2}}{g_{i22}}\\ &=e_{i2}\theta_{i1}^{*T}\varphi_{i1}+e_{i2}(\omega_{i1}+\omega_{iV})-\frac{e_{i2}^2\hat{\chi}_{i1}\varphi_{i1}^T\varphi_{i1}}{2\xi_{2i}^2}-\frac{e_{i2}^2\hat{\chi}_{i2}}{2\xi_{3i}^2}+e_{i2}e_{iT}g_{iV}-k_{i21}e_{i2}^2-k_{i22}sig^{r_i+1}(e_{i2})-\frac{\tilde{\chi}_{i1}\dot{\hat{\chi}}_{i1}}{g_{i12}}-\frac{\tilde{\chi}_{i2}\dot{\hat{\chi}}_{i2}}{g_{i22}}\end{aligned} \tag{46}$$

It can be found that $e_{i2}\theta_{i1}^{*T}\varphi_{i1}\le\left(e_{i2}^2\chi_{i1}\varphi_{i1}^T\varphi_{i1}/2\xi_{2i}^2\right)+\left(\xi_{2i}^2/2\right)$ and $e_{i2}(\omega_{i1}+\omega_{iV})\le\left(e_{i2}^2\chi_{i2}/2\xi_{3i}^2\right)+\left(\xi_{3i}^2/2\right)$ by using Young's inequality. Then, taking virtual control law (25) into (46), one has

$$\begin{aligned}\dot{V}_{i2}&\le -k_{i21}e_{i2}^2-k_{i22}sig^{r_i+1}(e_{i2})+\frac{\xi_{2i}^2}{2}+\frac{\xi_{3i}^2}{2}+e_{i2}e_{iT}g_{iV}+h_{i21}\hat{\chi}_{i1}\tilde{\chi}_{i1}+h_{i22}\hat{\chi}_{i2}\tilde{\chi}_{i2}\\ &\le -k_{i21}e_{i2}^2-k_{i22}sig^{r_i+1}(e_{i2})+\frac{\xi_{2i}^2}{2}+\frac{\xi_{3i}^2}{2}+e_{i2}e_{iT}g_{iV}-\frac{h_{i21}}{2}\tilde{\chi}_{i1}^2-\frac{h_{i22}}{2}\tilde{\chi}_{i2}^2+\frac{h_{i21}}{2}\chi_{i1}^2+\frac{h_{i22}}{2}\chi_{i2}^2\end{aligned}. \tag{47}$$

Recalling the virtual input (27), the time derivative of V_{i3} is

$$\begin{aligned}\dot{V}_{i3}&=e_{iT}\left(\dot{T}_i-\dot{\bar{T}}_i-\dot{\zeta}_{i1}\right)-\frac{\tilde{\chi}_{i3}\dot{\hat{\chi}}_{i3}}{g_{i23}}\\ &=e_{iT}\left(-k_{i24}e_{iT}-g_{iV}e_{i2}+\omega_{iT}-\frac{e_{iT}\hat{\chi}_{i3}}{2\xi_{i4}^2}\right)-\frac{\tilde{\chi}_{i3}\dot{\hat{\chi}}_{i3}}{g_{i23}}\end{aligned}. \tag{48}$$

By using Young's inequality, it can be seen that $e_{iT}\omega_{iT}\le e_{iT}^2\chi_{i3}/2\xi_{4i}^2+\xi_{4i}^2/2$. (48) can be rewritten as

$$\begin{aligned}\dot{V}_{i3}&\le -k_{i24}e_{iT}^2-g_{iV}e_{iT}e_{i2}+\frac{e_{iT}^2\chi_{i3}}{2\xi_{4i}^2}-\frac{e_{iT}^2\hat{\chi}_{i3}}{2\xi_{4i}^2}+\frac{\xi_{4i}^2}{2}-\frac{\tilde{\chi}_{i3}\dot{\hat{\chi}}_{i3}}{g_{i23}}\\ &\le -k_{i24}e_{iT}^2-g_{iV}e_{iT}e_{i2}+\frac{\xi_{4i}^2}{2}+\frac{h_{i23}}{2}\chi_{i3}^2-\frac{h_{i23}}{2}\tilde{\chi}_{i3}^2\end{aligned}. \tag{49}$$

STEP 3: The stability analysis of the flight path angle subsystem

Thirdly, choose the Lyapunov functions for the flight path angle subsystem as

$$\begin{cases} V_{i4} = \widehat{V}_i^2\left(\frac{1}{2}e_{i4}^2 + \frac{1}{2g_{i31}}\tilde{\chi}_{i4}^2 + \frac{1}{2g_{i32}}\tilde{\chi}_{i5}^2\right) \\ V_{i5} = \widehat{V}_i^2\left(\frac{1}{2}e_{i5}^2 + \frac{1}{2g_{i33}}\tilde{\chi}_{i6}^2 + \frac{1}{2g_{i34}}\tilde{\chi}_{i7}^2\right) \\ V_{i6} = \widehat{V}_i^2\left(\frac{1}{2}e_{i6}^2 + \frac{1}{2g_{i35}}\tilde{\chi}_{i8}^2 + \frac{1}{2g_{i36}}\tilde{\chi}_{i9}^2\right) \end{cases} \tag{50}$$

$$V_{i7} = \widehat{V}_i^2\left(\frac{1}{2}e_{i\delta}^2 + \frac{1}{2g_{i37}}\tilde{\chi}_{i10}^2\right) \tag{51}$$

where $\tilde{\chi}_{ip} = \chi_{ip} - \hat{\chi}_{ip}$ is the estimation error for $p \in \{4, 5, \ldots, 10\}$. The time derivatives of V_{i4}, V_{i5} and V_{i6} are

$$\begin{cases} \dot{V}_{i4} = \widehat{V}_i^2\left(e_{i4}\left(f_{i2} + \bar{x}_{i5} - \dot{\bar{x}}_{i4}\right) - \frac{\tilde{\chi}_{i4}\dot{\hat{\chi}}_{i4}}{g_{i31}} - \frac{\tilde{\chi}_{i5}\dot{\hat{\chi}}_{i5}}{g_{i32}}\right) \\ \dot{V}_{i5} = \widehat{V}_i^2\left(e_{i5}\left(f_{i3} + \bar{x}_{i6} - \dot{\bar{x}}_{i5}\right) - \frac{\tilde{\chi}_{i6}\dot{\hat{\chi}}_{i6}}{g_{i33}} - \frac{\tilde{\chi}_{i7}\dot{\hat{\chi}}_{i7}}{g_{i34}}\right) \\ \dot{V}_{i6} = \widehat{V}_i^2\left(e_{i6}\left(f_{i4} + \bar{\delta}_{ie} - \dot{\bar{x}}_{i6}\right) - \frac{\tilde{\chi}_{i8}\dot{\hat{\chi}}_{i8}}{g_{i35}} - \frac{\tilde{\chi}_{i9}\dot{\hat{\chi}}_{i9}}{g_{i36}}\right) \end{cases} \tag{52}$$

Due to the space limitations and similarity of derivation, only the detailed derivation of $\dot{V}_{i4}$ is shown in this paper. The derivation of $\dot{V}_{i5}$ and $\dot{V}_{i6}$ are totally the same as the derivation of $\dot{V}_{i4}$. Consider the RBFNN $f_2 = \theta_{i2}^{*T}\varphi_{i2} + \omega_{i2} + \omega_{i\alpha f}$ and (31), $\dot{V}_{i4}$ can be rewritten as

$$\begin{aligned} \dot{V}_{i4} &= \widehat{V}_i^2\left(e_{i4}\left(\theta_{i2}^{*T}\varphi_{i2} + \omega_{i2} + \omega_{i\alpha f} + \bar{x}_{i5} + e_{i5} - \dot{\bar{x}}_{i4}\right) - \frac{\tilde{\chi}_{i4}\dot{\hat{\chi}}_{i4}}{g_{i31}} - \frac{\tilde{\chi}_{i5}\dot{\hat{\chi}}_{i5}}{g_{i32}}\right) \\ &= \widehat{V}_i^2\left(e_{i4}\theta_{i2}^{*T}\varphi_{i2} + e_{i4}(\omega_{i2} + \omega_{i\alpha f} + \omega_{i\gamma}) - \frac{e_{i4}^2\hat{\chi}_{i4}\varphi_{i2}^T\varphi_{i2}}{2\xi_{5i}^2} - \frac{e_{i4}^2\hat{\chi}_{i5}}{2\xi_{6i}^2} + e_{i4}e_{i5} - k_{i31}e_{i4}^2 - k_{i32}sig^{r_i+1}(e_{i4}) - \frac{\tilde{\chi}_{i4}\dot{\hat{\chi}}_{i4}}{g_{i31}} - \frac{\tilde{\chi}_{i5}\dot{\hat{\chi}}_{i5}}{g_{i32}}\right) \end{aligned} \tag{53}$$

It can be found that $e_{i4}\theta_{i2}^{*T}\varphi_{i2} \le \left(e_{i4}^2\chi_{i4}\varphi_{i2}^T\varphi_{i2}/2\xi_{5i}^2\right) + \left(\xi_{5i}^2/2\right)$ and $e_{i4}(\omega_{i2} + \omega_{i\alpha f} + \omega_{i\gamma}) \le \left(e_{i4}^2\chi_{i5}/2\xi_{6i}^2\right) + \left(\xi_{6i}^2/2\right)$ by using Young's inequality. Taking the adaptive law (32) and (33) into (53), one has

$$\begin{aligned} \dot{V}_{i4} &\le \widehat{V}_i^2\left(\frac{e_{i4}^2\chi_{i4}\varphi_{i2}^T\varphi_{i2}}{2\xi_{5i}^2} + \frac{\xi_{5i}^2}{2} + \frac{e_{i4}^2\chi_{i5}}{2\xi_{6i}^2} + \frac{\xi_{6i}^2}{2} - \frac{e_{i4}^2\hat{\chi}_{i4}\varphi_{i2}^T\varphi_{i2}}{2\xi_{5i}^2} - \frac{e_{i4}^2\hat{\chi}_{i5}}{2\xi_{6i}^2} + e_{i4}e_{i5} - k_{i31}e_{i4}^2 - k_{i32}sig^{r_i+1}(e_{i4}) - \frac{\tilde{\chi}_{i4}\dot{\hat{\chi}}_{i4}}{g_{i31}} - \frac{\tilde{\chi}_{i5}\dot{\hat{\chi}}_{i5}}{g_{i32}}\right) \\ &= \widehat{V}_i^2\left(-k_{i31}e_{i4}^2 - k_{i32}sig^{r_i+1}(e_{i4}) + e_{i4}e_{i5} + \frac{\xi_{5i}^2}{2} + \frac{\xi_{6i}^2}{2} + h_{i31}\tilde{\chi}_{i4}\hat{\chi}_{i4} + h_{i32}\tilde{\chi}_{i5}\hat{\chi}_{i5}\right) \\ &\le \widehat{V}_i^2\left(-k_{i31}e_{i4}^2 - k_{i32}sig^{r_i+1}(e_{i4}) + e_{i4}e_{i5} + \frac{\xi_{5i}^2}{2} + \frac{\xi_{6i}^2}{2} - \frac{h_{i31}}{2}\tilde{\chi}_{i4}^2 - \frac{h_{i32}}{2}\tilde{\chi}_{i5}^2 + \frac{h_{i31}}{2}\chi_{i4}^2 + \frac{h_{i32}}{2}\chi_{i5}^2\right) \end{aligned} \tag{54}$$

According to the same derivation, it is easy to be obtained that

$$\begin{cases} \dot{V}_{i5} \le \widehat{V}_i^2\left(-k_{i33}e_{i5}^2 - k_{i34}sig^{r_i+1}(e_{i5}) + e_{i5}e_{i6} - e_{i4}e_{i5} + \frac{\xi_{7i}^2}{2} + \frac{\xi_{8i}^2}{2} - \frac{h_{i33}}{2}\tilde{\chi}_{i6}^2 - \frac{h_{i34}}{2}\tilde{\chi}_{i7}^2 + \frac{h_{i33}}{2}\chi_{i6}^2 + \frac{h_{i34}}{2}\chi_{i7}^2\right) \\ \dot{V}_{i6} \le \widehat{V}_i^2\left(-k_{i35}e_{i6}^2 - k_{i36}sig^{r_i+1}(e_{i6}) + e_{i6}e_{i\delta} - e_{i5}e_{i6} + \frac{\xi_{9i}^2}{2} + \frac{\xi_{10i}^2}{2} - \frac{h_{i35}}{2}\tilde{\chi}_{i8}^2 - \frac{h_{i36}}{2}\tilde{\chi}_{i9}^2 + \frac{h_{i35}}{2}\chi_{i8}^2 + \frac{h_{i36}}{2}\chi_{i9}^2\right) \end{cases} \tag{55}$$

Recalling the virtual input (35), the time derivative of V_{i7} is

$$\begin{aligned} \dot{V}_{i7} &= \widehat{V}_i^2\left(e_{i\delta}\left(\dot{\delta}_{ie} - \dot{\bar{\delta}}_{ie} - \dot{\zeta}_{i2}\right) - \frac{\tilde{\chi}_{i10}\dot{\hat{\chi}}_{i10}}{g_{i37}}\right) \\ &= \widehat{V}_i^2\left(e_{i\delta}\left(-k_{i38}e_{i\delta} - e_{i6} - \frac{e_{i\delta}\hat{\chi}_{i10}}{2\xi_{i11}^2} + \omega_{i\delta}\right) - \frac{\tilde{\chi}_{i10}\dot{\hat{\chi}}_{i10}}{g_{i37}}\right) \end{aligned} \tag{56}$$

By using Young's inequality, it can be seen that $e_{i\delta}\omega_{i\delta} \le e_{i\delta}^2\chi_{i10}/2\xi_{11i}^2 + \xi_{11i}^2/2$, where $\chi_{i10} = \bar{\omega}_{i\delta}^2$. (56) can be rewritten as

$$\begin{aligned}\dot{V}_{i7} &\le \widehat{V}_i^2\left(-k_{i38}e_{i\delta}^2 - e_{i6}e_{i\delta} + \frac{e_{i\delta}\chi_{i10}}{2\xi_{i11}^2} + \frac{\xi_{11i}^2}{2} - \frac{e_{i\delta}\hat{\chi}_{i10}}{2\xi_{i11}^2} - \frac{\tilde{\chi}_{i10}\dot{\hat{\chi}}_{i10}}{g_{i37}}\right)\\ &\le \widehat{V}_i^2\left(-k_{i38}e_{i\delta}^2 - e_{i6}e_{i\delta} + \frac{\xi_{11i}^2}{2} + \frac{h_{i37}}{2}\chi_{i10}^2 - \frac{h_{i37}}{2}\tilde{\chi}_{i10}^2\right)\end{aligned}. \tag{57}$$

STEP 4: The stability analysis of the whole UAV system

Finally, consider the following Lyapunov function candidate of the whole UAV system as

$$V_{iall} = V_{i1} + V_{i2} + V_{i3} + V_{i4} + V_{i5} + V_{i6} + V_{i7}. \tag{58}$$

The time derivative of (58) is

$$\begin{aligned}\dot{V}_{iall} \le &-\left(k_{i11} - \frac{3(2\tau_i+1)^2}{2\xi_{1i}^2}\right)S_{ie}^T S_{ie} - k_{i12}S_{ie}^T sig^{r_i}(S_{ie}) - \left(k_{i13} - \frac{3}{2\xi_{1i}^2}\right)\varepsilon_i^2 - k_{i14}sig^{r_i+1}(\varepsilon_i) - \left(k_{i21} - \frac{\xi_{1i}^2}{2}\right)e_{i2}^2\\ &- k_{i22}sig^{r_i+1}(e_{i2}) - k_{i24}e_{iT}^2 + \sum_{j=2}^{4}\frac{\xi_{ji}^2}{2} + \sum_{j=1}^{3}\left(\frac{h_{i2j}}{2}\chi_{ij}^2 - \frac{h_{i2j}}{2}\tilde{\chi}_{ij}^2\right) + \widehat{V}_i^2\left(-\left(k_{i31} - \frac{\xi_{1i}^2}{2}\right)e_{i4}^2 - k_{i32}sig^{r_i+1}(e_{i4}) - k_{i33}e_{i5}^2\right.\\ &\left.-k_{i34}sig^{r_i+1}(e_{i5}) - k_{i35}e_{i6}^2 - k_{i36}sig^{r_i+1}(e_{i6}) - k_{i38}e_{i\delta}^2 + \sum_{j=5}^{11}\frac{\xi_{ji}^2}{2} + \sum_{j=1}^{7}\left(\frac{h_{3j}}{2}\chi_{i(j+3)}^2 - \frac{h_{3j}}{2}\tilde{\chi}_{i(j+3)}^2\right)\right)\\ &\le \upsilon_i V_{iall} + \varsigma_i\end{aligned} \tag{59}$$

where $\upsilon_i = \min\{2\left(k_{i11} - 3(2\tau_i+1)^2/2\xi_{1i}^2\right), 2\left(k_{i13} - 3/2\xi_{1i}^2\right), 2\left(k_{i21} - \xi_{1i}^2/2\right), 2k_{i24}, 2\left(k_{i31} - \xi_{1i}^2/2\right), 2k_{i33}, 2k_{i35}, 2k_{i38}, h_{i21}, h_{i22}, h_{i23}, h_{i31}, h_{i32}, h_{i33}, h_{i34}, h_{i35}, h_{i36}, h_{i37}\}$ and $\varsigma_i = \sum_{j=2}^{4}\xi_{ji}^2/2 + \sum_{j=1}^{3}h_{i(2j)}\chi_{ij}^2/2 + \widehat{V}_i^2\left(\sum_{j=5}^{11}\xi_{ji}^2/2 + \sum_{j=1}^{7}h_{3j}\chi_{i(j-3)}^2/2\right)$. If the control parameters are chosen well, then S_{ie}, ε_i, e_{i2}, e_{i4}, e_{i5}, e_{i6}, e_{iT}, $e_{i\delta}$ and $\tilde{\chi}_{ij}$ for $j \in \{1, 2, \ldots, 10\}$ are bounded because of the boundedness theorem. Consider $\tilde{\chi}_{ij} \le \bar{\chi}_{ij}$ for $j \in \{1, 2, \ldots, 10\}$ where $\bar{\chi}_{ij}$ is the upper bound on the estimation error. Subsequently, another Lyapunov function candidate is used to analyze the finite-time stability

$$V_{if} = V_{S_{ie}} + \frac{1}{2}\varepsilon_i^2 + \frac{1}{2}e_{i2}^2 + \frac{\widehat{V}_i^2}{2}e_{i4}^2 + \frac{\widehat{V}_i^2}{2}e_{i5}^2 + \frac{\widehat{V}_i^2}{2}e_{i6}^2. \tag{60}$$

Taking the time derivative of V_{if} gives that

$$\begin{aligned}\dot{V}_{if} \le &-\left(k_{i11} - \frac{3(2\tau_i+1)^2}{2\xi_{1i}^2}\right)S_{ie}^T S_{ie} - k_{i12}S_{ie}^T sig^{r_i}(S_{ie}) - \left(k_{i21} - \frac{\xi_{1i}^2}{2} - \frac{\bar{\chi}_{i1}\varphi_{i1}^T\varphi_{i1}}{2\xi_{2i}^2} - \frac{\bar{\chi}_{i2}}{2\xi_{3i}^2} - \frac{1}{2}\right)e_{i2}^2\\ &- \left(k_{i13} - \frac{3}{2\xi_{1i}^2}\right)\varepsilon_i^2 - k_{i14}sig^{r_i+1}(\varepsilon_i) - k_{i22}sig^{r_i+1}(e_{i2}) + \widehat{V}_i^2\left(-k_{i32}sig^{r_i+1}(e_{i4}) - \left(k_{i31} - \frac{\xi_{1i}^2}{2} - \frac{\bar{\chi}_{i4}\varphi_{i2}^T\varphi_{i2}}{2\xi_{5i}^2} - \frac{\bar{\chi}_{i5}}{2\xi_{6i}^2}\right)e_{i4}^2\right.\\ &\left.- \left(k_{i33} - \frac{\bar{\chi}_{i6}\varphi_{i3}^T\varphi_{i3}}{2\xi_{7i}^2} - \frac{\bar{\chi}_{i7}}{2\xi_{8i}^2}\right)e_{i5}^2 - k_{i34}sig^{r_i+1}(e_{i5}) - \left(k_{i35} - \frac{\bar{\chi}_{i8}\varphi_{i4}^T\varphi_{i4}}{2\xi_{9i}^2} - \frac{\bar{\chi}_{i9}}{2\xi_{10i}^2} - \frac{1}{2}\right)e_{i6}^2 - k_{i36}sig^{r_i+1}(e_{i6})\right) + \varsigma_{if}\end{aligned} \tag{61}$$

where $\varsigma_{if} = \sum_{j=2}^{4}\xi_{ji}^2/2 + e_{iT}^2/2 + \widehat{V}_i^2\left(\sum_{j=5}^{11}\xi_{ji}^2/2 + e_{i\delta}^2/2\right)$.

Then, we can get that

$$\begin{aligned}\dot{V}_{if} &\le -\lambda_{\min}(\mathbf{P}_i)V_{if} - \lambda_{\min}(\mathbf{Q}_i)m_{ir}\left[V_{S_{ie}}^{\frac{(r_i+1)}{2}} + \left(\frac{1}{2}\varepsilon_i^2\right)^{\frac{(r_i+1)}{2}} + \left(\frac{1}{2}e_{i2}^2\right)^{\frac{(r_i+1)}{2}} + \left(\frac{\widehat{V}_i^2}{2}e_{i4}^2\right)^{\frac{(r_i+1)}{2}}\right.\\ &\left. + \left(\frac{\widehat{V}_i^2}{2}e_{i5}^2\right)^{\frac{(r_i+1)}{2}} + \left(\frac{\widehat{V}_i^2}{2}e_{i6}^2\right)^{\frac{(r_i+1)}{2}}\right] + \varsigma_{if}\\ &\le -\lambda_{\min}(\mathbf{P}_i)V_{if} - \lambda_{\min}(\mathbf{Q}_i)m_{ir}V_{if}^{\frac{(r_i+1)}{2}} + \varsigma_{if}\end{aligned} \tag{62}$$

where $m_{ir} = \min\{2^{(r_i-1)/2}, 2^{(r_i-1)/2}/\widehat{V}_i^{(r_i-1)}\}$, $\mathbf{Q}_i = diag\{2k_{i12}, 2k_{i14}, 2k_{i22}, 2k_{i32}, 2k_{i34}, 2k_{i36}\}$ and $\mathbf{P}_i = diag\{2\left(k_{i11} - 3(2\tau_i+1)^2/2\xi_{1i}^2\right), 2\left(k_{i13} - 3/2\xi_{1i}^2\right), 2\left(k_{i21} - \xi_{1i}^2/2 - \bar{\chi}_{i1}\varphi_{i1}^T\varphi_{i1}/2\xi_{2i}^2 - \bar{\chi}_{i2}/2\xi_{3i}^2 - 1/2\right), 2\widehat{V}_i^2\left(k_{i31} - \xi_{1i}^2/2 - \bar{\chi}_{i4}\varphi_{i2}^T\varphi_{i2}/2\xi_{5i}^2 - \bar{\chi}_{i5}/2\xi_{6i}^2\right), 2\widehat{V}_i^2\left(k_{i33} - \bar{\chi}_{i6}\varphi_{i3}^T\varphi_{i3}/2\xi_{7i}^2 - \bar{\chi}_{i7}/2\xi_{8i}^2\right), 2\widehat{V}_i^2\left(k_{i35} - \bar{\chi}_{i8}\varphi_{i4}^T\varphi_{i4}/2\xi_{9i}^2 - \bar{\chi}_{i9}/2\xi_{10i}^2 - 1/2\right)\}$. According to Lemma 1, if the parameters satisfy

Table 1
Initial states of the UAVs.

	UAV1	UAV2	UAV3	UAV4
$p_i(0)$	$[-8,-8]$	$[-10,4]$	$[-12,3]$	$[-9,12]$
$\dot{p}_i(0)$	$[30,0]$	$[30,0]$	$[30,0]$	$[30,0]$
d_{il}	$[2.5,-5]$	$[2.5,5]$	$[-2.5,0]$	$[-2.5,10]$

$$\begin{cases} k_{i11} > \dfrac{3(2\tau_i+1)^2}{2\xi_{1i}^2} \\ k_{i13} > \dfrac{3}{2\xi_{1i}^2} \\ k_{i21} > \dfrac{\xi_{1i}^2}{2} + \dfrac{\bar{\chi}_{i1}\varphi_{i1}^T\varphi_{i1}}{2\xi_{2i}^2} + \dfrac{\bar{\chi}_{i2}}{2\xi_{3i}^2} + \dfrac{1}{2} \\ k_{i31} > \dfrac{\xi_{1i}^2}{2} + \dfrac{\bar{\chi}_{i4}\varphi_{i2}^T\varphi_{i2}}{2\xi_{5i}^2} + \dfrac{\bar{\chi}_{i5}}{2\xi_{6i}^2} \\ k_{i33} > \dfrac{\bar{\chi}_{i6}\varphi_{i3}^T\varphi_{i3}}{2\xi_{7i}^2} + \dfrac{\bar{\chi}_{i7}}{2\xi_{8i}^2} \\ k_{i35} > \dfrac{\bar{\chi}_{i8}\varphi_{i4}^T\varphi_{i4}}{2\xi_{9i}^2} + \dfrac{\bar{\chi}_{i9}}{2\xi_{10i}^2} + \dfrac{1}{2} \end{cases}, \tag{63}$$

the tracking errors of the states $E_{iall} = \{\varepsilon_i, e_{i2}, e_{i4}, e_{i5}, e_{i6}, S_{ie}\}$ will converge to the bounded set $\Omega_i = \min\{\Omega_{i1}, \Omega_{i2}\}$ in a finite time $t_{i1} = \max\{t_{if1}, t_{if2}\}$, where

$$\begin{cases} t_{if1} \le \dfrac{2}{\vartheta_i\lambda_{\min}(\mathbf{P}_i)(1-r_i)} \ln\left(\dfrac{\vartheta_i\lambda_{\min}(\mathbf{P}_i) V_{if}^{(1-r_i)/2}(t_0) + \lambda_{\min}(\mathbf{Q}_i) m_{ir}}{\lambda_{\min}(\mathbf{Q}_i) m_{ir}}\right) \\ t_{if2} \le \dfrac{2}{\lambda_{\min}(\mathbf{P}_i)(1-r_i)} \ln\left(\dfrac{\lambda_{\min}(\mathbf{P}_i) V_{if}^{(1-r_i)/2}(t_0) + \vartheta_i\lambda_{\min}(\mathbf{Q}_i) m_{ir}}{\vartheta_i\lambda_{\min}(\mathbf{Q}_i) m_{ir}}\right) \end{cases}, \tag{64}$$

$$\begin{cases} \Omega_{i1} = \left\{x_i \in E_i : V_{if} \le (\sigma_i/(1-\vartheta_i)\lambda_{\min}(\mathbf{P}_i))\right\} \\ \Omega_{i2} = \left\{x_i \in E_i : V_{if}^{(r_i+1)/2} \le (\sigma_i/(1-\vartheta_i)\lambda_{\min}(\mathbf{Q}_i) m_{ir})\right\} \end{cases}. \tag{65}$$

Furthermore, the transformed error S_{ie} is bounded means that the ith UAV will converge to the neighbor of the desired formation position in a finite time. From (62), it can be obtained that the (Textranslationfailed) and S_{ie} can converge to a small neighborhood of the origin if $\lambda_{\min}(\mathbf{P}_i)$ and $\lambda_{\min}(\mathbf{Q}_i)$ are large enough which can be achieved by setting parameters properly.

According to that e_{i2} and e_{i4} are bounded, one can assume that $\left(\xi_{1i}^2 \left\|\tilde{p}_{i2}[1]\right\|_2^2 + \xi_{1i}^2 \bar{V}_i^2 \left\|\tilde{p}_{i2}[2]\right\|_2^2\right)/2 \le \eta_{\max}$. By setting the parameters k_{i11}, k_{i12}, k_{i13}, k_{i14} and ξ_{1i} properly, it can be guaranteed that $-\lambda_{\min}(\mathbf{P}_{is}) V_{i1}(0) - 2^{(r_i-1)/2}\lambda_{\min}(\mathbf{Q}_{is}) V_{i1}^{(r_i+1)/2}(0) < -\eta_{\max}$, where $\mathbf{P}_{is} = diag\left\{2\left(k_{i11} - 3(2\tau_i+1)^2/\left(2\xi_{1i}^2\right)\right), 2\left(k_{i13} - 3/2\xi_{1i}^2\right)\right\}$ and $\mathbf{Q}_{is} = diag\{2k_{i12}, 2k_{i14}\}$. Thus, by combining (42), it can be seen that $\dot{V}_{i1}(0) < 0$ such that $V_{i1}(t) < V_{i1}(0)$ as mentioned in Remark 3. Specifically, $V_{i1}(t)$ is bounded in $\Omega_{ip} = \{V_{i1} : V_{i1} \le c_{ip}\}$, where $c_{ip} < V_{i1}(0)$. Up to now, the proof that the ith UAV will move in $\Omega_{ib}(t)$ under the control law designed in this paper is completed.

Remark 5. By limiting the flight of the UAV in the designated region, not only can the collisions be avoided, but also some obstacles with small radius can be avoided by making them cross the gaps between UAVs in the formation. This is also the research direction of our future work.

4. Examples

A team of 4 follower UAVs with a virtual leader is taken into consideration and each follower UAV can get the information about the leader by the fixed-time HODO in [47]. The purpose of the task is to form a diamond formation whose details are listed in Table 1. The structure parameters and coefficient values of UAVs can be referred to [25]. The input saturation limits of the UAVs are $T_i \in (0, 120)$ and $\delta_{ie} \in (-0.8, 0.8)$. The initial position and the velocity of the virtual leader are $p_l(0) = [10, 0]^T$ and $\dot{p}_l(t) = [30, 0.1\sin(0.2t)]^T$. The initial states of follower UAVs and d_{il} are shown in Table 1.

The initial states of the adaptive laws and the input signals are set as zeros. The initial states of differentiators are set as zeros. The BLFs are chosen as $1/\left(s^2 + 1.414s + 1\right)$ [44]. The RBFNN is used to approximate f_{i1}, f_{i2}, f_{i3} and f_{i4} contains ten nodes for $(V_i, \alpha_i, \gamma_i, T_i, \delta_{ie}, q_i)$ with centers evenly spaced in $[20, 40] \times [-0.4, 0.4] \times [-0.4, 0.4] \times [0, 120] \times [-1, 1] \times [-0.4, 0.4]$. The neural cell widths are chosen about 18. The control parameters for the position subsystem are designed as $\omega_{i0} = 0.5$, $\omega_{i\infty} = 0.05$, $k_{i1} = [k_{i11}, k_{i12}, k_{i13}, k_{i14}, k_{i15}] = [5, 0.8, 5, 0.3, 3]$ and $\xi_{1i} = 4$. The control parameters for the velocity subsystem are designed as $k_{i2} = [k_{i21}, k_{i22}, k_{i23}, k_{i24}, k_{i25}] = [1, 0.5, 1, 5, 2]$, $h_{i2} = [h_{i21}, h_{i22}, h_{i23}] = [0.05, 0.01, 0.01]$ and $g_{i2} = [g_{i21}, g_{i22}, g_{i23}] = [2, 0.7, 0.01]$. The control parameters for the flight

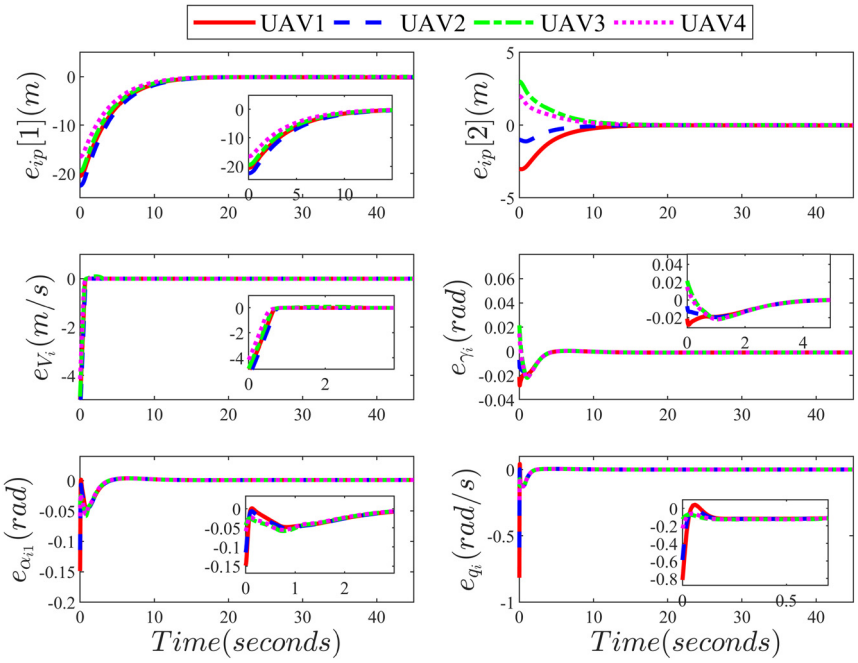

Fig. 5. Tracking errors of the follower UAVs.

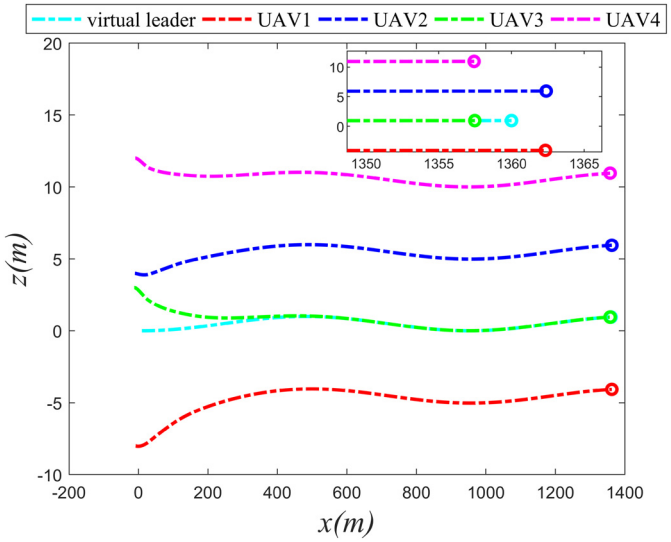

Fig. 6. The flight trajectories of follower UAVs. (For interpretation of the colors in the figure(s), the reader is referred to the web version of this article.)

path angle subsystem are designed as $k_{i3} = [k_{i31}, k_{i32}, k_{i33}, k_{i34}, k_{i35}, k_{i36}] = [1, 1, 0.3, 0.3, 2, 3]$, $h_{i3} = [h_{i31}, h_{i32}, h_{i33}, h_{i34}, h_{i35}, h_{i36}, h_{i37}] = [0.5, 0.1, 0.5, 0.1, 0.2, 0.1, 0.051]$ and $g_{i3} = [g_{i31}, g_{i32}, g_{i33}, g_{i34}, g_{i35}, g_{i36}, g_{i37}] = [1, 0.2, 1, 0.5, 3, 0.5, 2]$.

In this subsection, the effectiveness of the proposed finite-time controller based on the backstepping method is verified from the simulations. It is clearly illustrated in Fig. 5 that the errors of all states of the follower UAVs are converged into the small neighborhood of the origin in a finite time, which proves the effectiveness of the finite-time controller. Fig. 6 and 7 show the trajectories of the follower UAVs where it can be seen that each UAV is contained in Ω_{ib} during the flight and eventually forms a diamond formation without collisions. In other words, the control scheme proposed in this paper is with global collision avoidance. Besides, they give a visual representation of Remark 3. In Fig. 8, by utilizing the prescribed performance method, it can be seen that the state l_i is contained within the designed prescribed performance set, which is as consistent as the theoretical analysis.

The curves in Fig. 9 describe the inputs of the follower UAVs. From the curves of T_i and δ_{ie} for $i \in \{1, 2, 3, 4\}$, it is observed that T_i nearly reaches the limit at the beginning and δ_{ie} is in the limit of the elevator deflection angles, which confirms the effectiveness of the dynamic system proposed in this paper. To make the point more obvious, the simulation without considering the input saturation problem is shown in Fig. 10. It verifies the merit of the dynamic system proposed in this paper. Fig. 11 shows the estimate values about the adaptive laws and Fig. 12 shows the estimate values about RBFNN by using MLPNN. It is easy to find that all of them are bounded.

In order to compare with the previous method to address the input saturation problem, some numerical simulations have been done based on the auxiliary system based controller (ASBC) [24,25], dynamic system based controller (DSBC) [27], and the improved dynamic

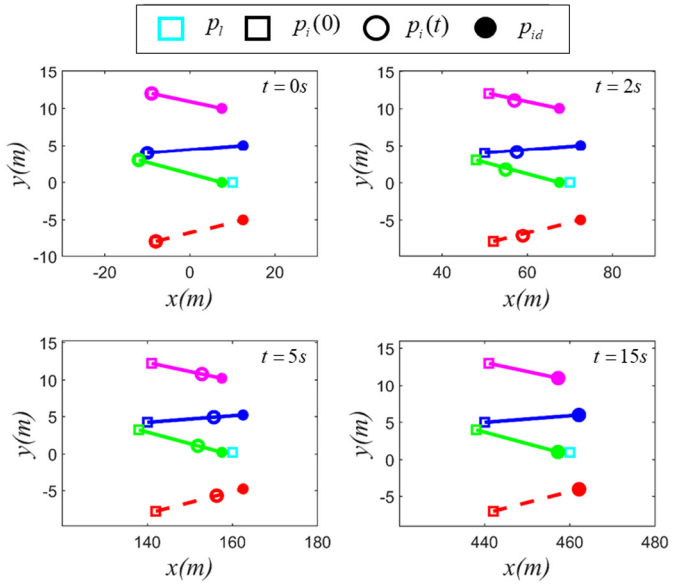

Fig. 7. The snapshots of the position of the follower UAVs.

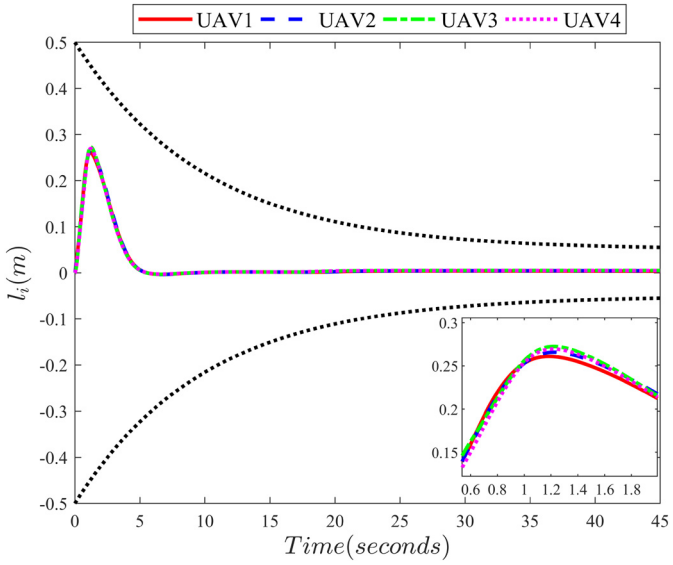

Fig. 8. Time response of the l_i.

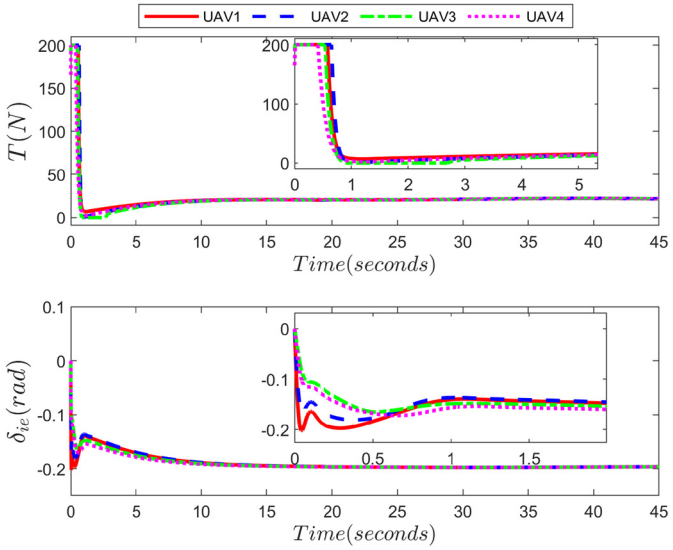

Fig. 9. Control inputs of the follower UAVs.

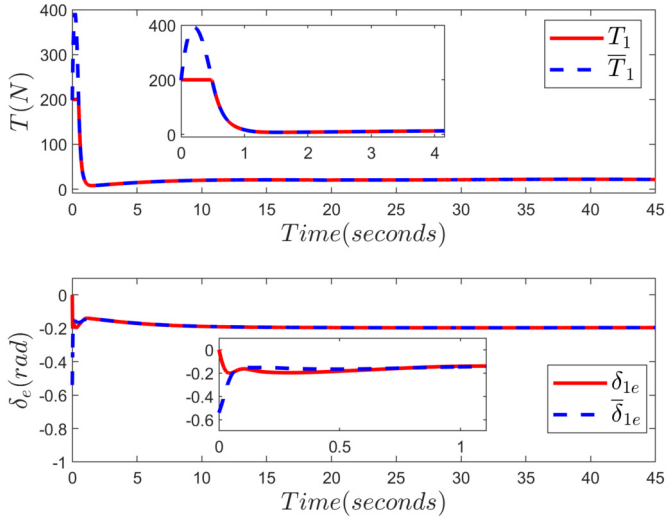

Fig. 10. The desired and limited control inputs of the 1st UAV.

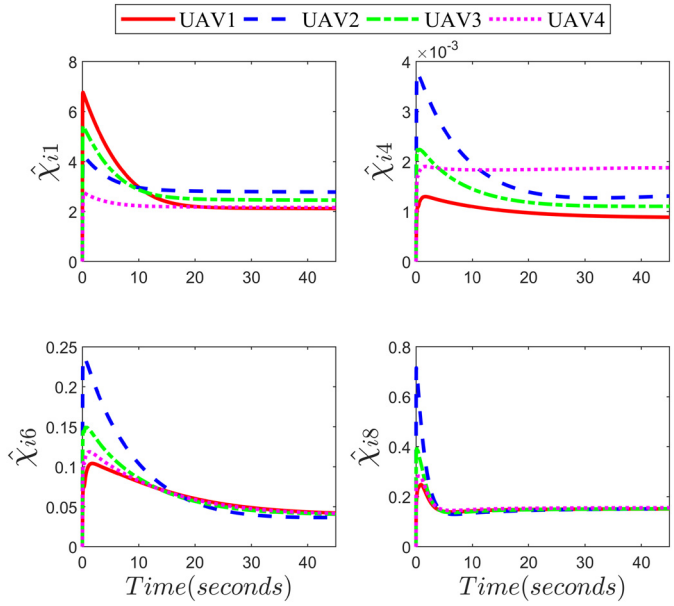

Fig. 11. MLPNN adaptive parameters.

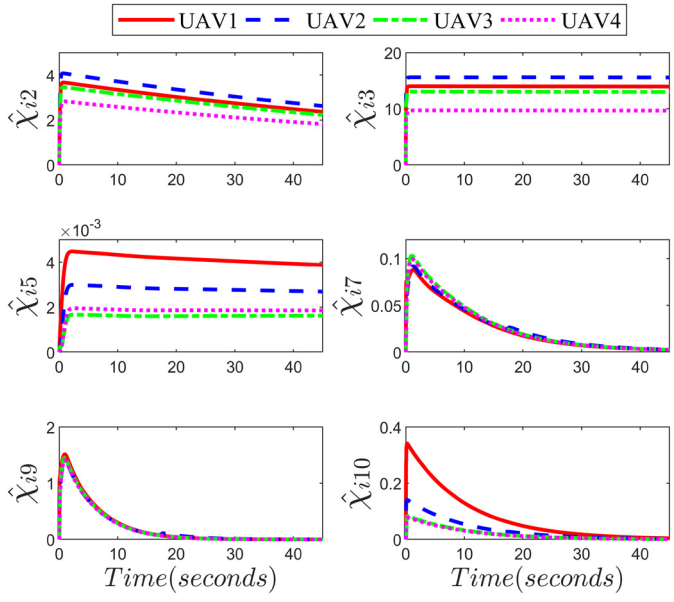

Fig. 12. Adaptive parameters.

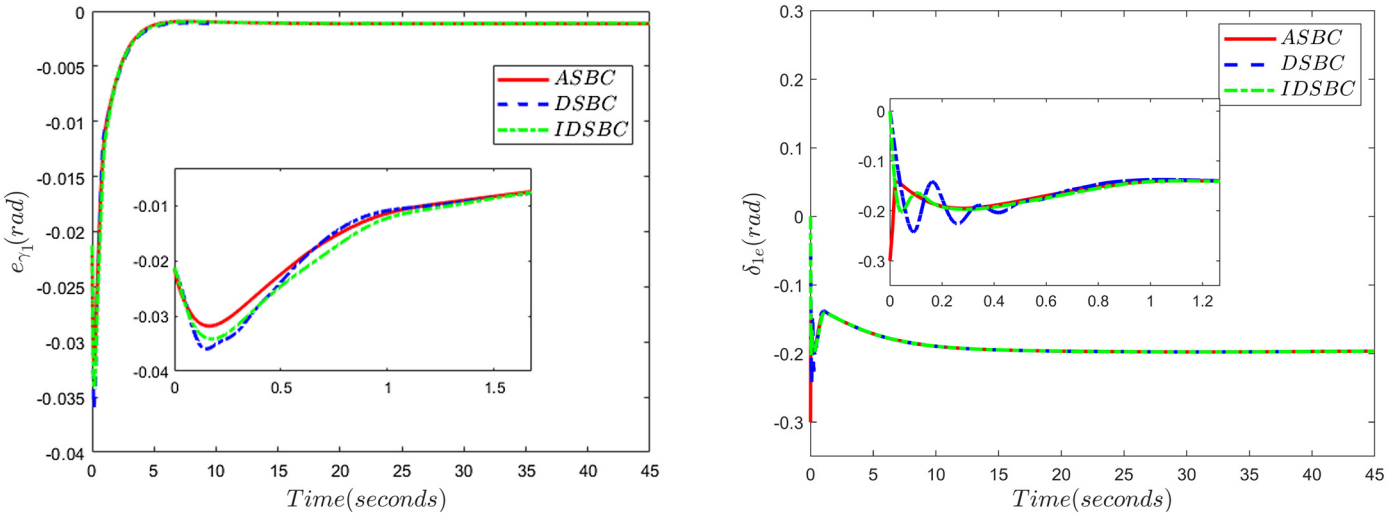

Fig. 13. $e_{\gamma 1}$ and δ_e under the ASBC, DSBC and IDSBC.

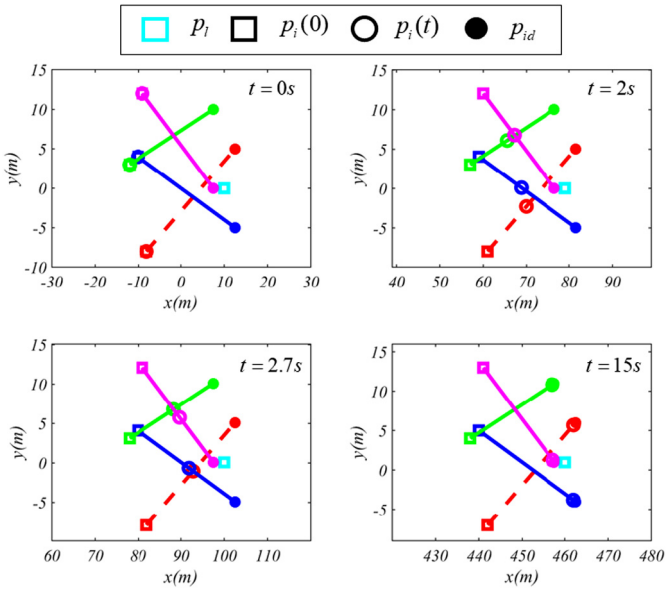

Fig. 14. The snapshots of the position of the follower UAVs without collision avoidance.

system based controller (IDSBC) presented in this paper, respectively. Since DSBC can only deal with the symmetry saturation problem, the flight path angle subsystem of the 1st UAV is considered as the comparison model. The simulation results are shown as follows.

From Fig. 13, it can be seen that the ASBC responds faster and has a better control effect since it is not affected by the initial value. The dynamic system can be considered as an integration system. Thus, the response speed of the dynamic system is not as fast as that of the ASBC system because of the characteristics of the integral system. However, ASBC also has its shortcomings as mentioned in Remark 4. Comparing DSBC and IDSBC, it is not difficult to find that the response of IDSBC is faster and smoother, and the control effect of IDSBC is better than DSBC. The simulation results reveal that the IDSBC constructed in this paper avoids the occurrence of the time-varying limit problem in DSBC [27].

To show the effectiveness of the collision avoidance algorithm more intuitively, the simulation results without formation reconstruction algorithm and collision avoidance are shown in Fig. 14. It shows that there are collisions between the 3rd follower and the 4th follower at 2 s. The 1st follower collides with the 2nd follower at 2.7 s. Compared with Fig. 7, it verifies the effectiveness of the collision avoidance algorithm in the paper.

An exquisite simulation is designed to verify that the collision avoidance algorithm proposed in this paper can avoid the problem of local minimum by using the APF. Two UAVs from the initial positions $[0, -10]$ and $[0, 10]$ will fly to the desired positions $[20, -5]$ and $[20, 5]$. From Fig. 15, it can be found that without Algorithm 1, the desired positions for UAVs may be allocated very unreasonably, resulting in the local minimum problem by using APF. Then, the UAVs will be stuck and cannot converge to the desired position. However, with the utilizing of the collision avoidance scheme in this paper, this problem will not arise.

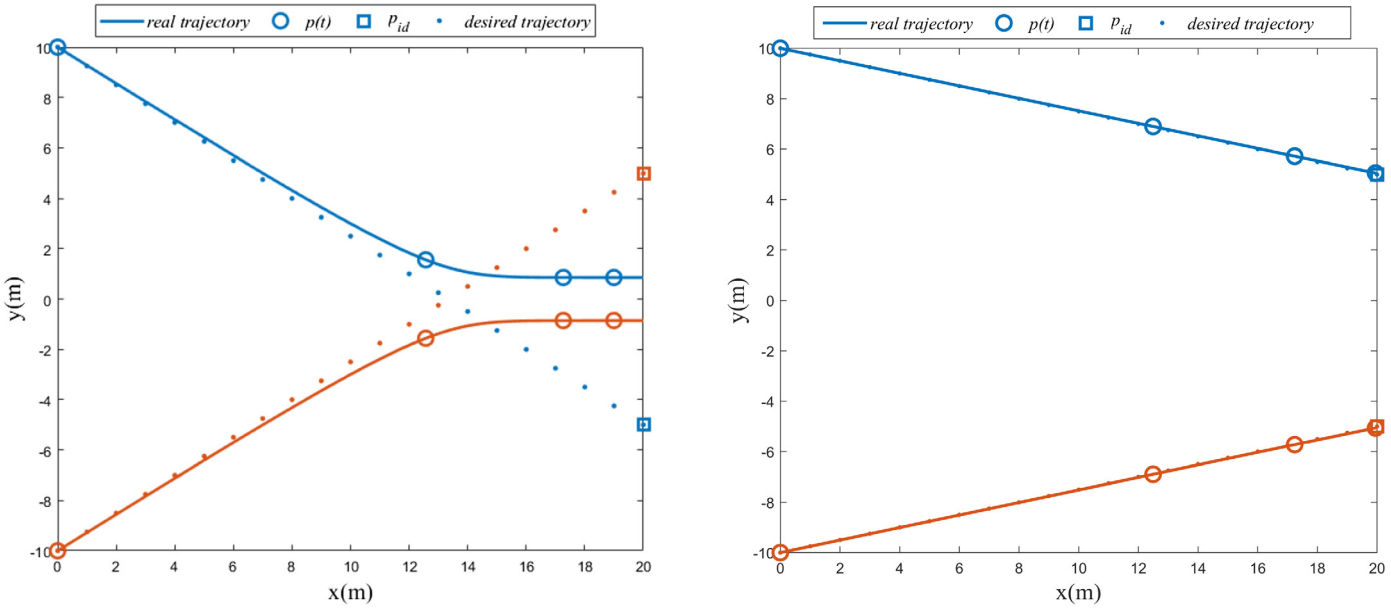

(a) APF (b) the method in this paper

Fig. 15. The snapshots of the follower UAVs with different collision avoidance methods.

5. Conclusion

The adaptive distributed finite-time control law with input saturation and unknown parameters for multi-UAVs is presented in this paper. Utilizing the control law proposed in this paper, the UAVs will converge in the small neighborhood of the desired position in finite time, and during this period, all UAVs will move in a specified region. Therefore, by combining the novel formation reconstruction algorithm, the control law can achieve global collision avoidance between UAVs without utilizing the distance-based method. Moreover, an improved auxiliary dynamic system governed by hyperbolic functions is constructed in this paper to overcome the shortcomings in the basic dynamic system and auxiliary system. The simulation results have revealed the superiority and effectiveness of the proposed control scheme. In the future, generalizing the results of the control law to three-dimensional space and employing this scheme to avoid obstacles are important research directions.

Declaration of competing interest

The authors declare that they have no known competing financial interests or personal relationships that could have appeared to influence the work reported in this paper.

Acknowledgements

This study was supported by the National Natural Science Foundation of China (No. 61803307, 62111530051), Aeronautical Science Foundation of China (No. 201901053004), Natural Science Basic Research Plan in Shaanxi Province of China (No. 2020JQ-209), China Postdoctoral Science Foundation (No. 2020M683565), and the Fundamental Research Funds for the Central Universities (No. 3102020ZDHKY05).

References

[1] B. Zhu, L. Xie, D. Han, X. Meng, R. Teo, A survey on recent progress in control of swarm systems, Sci. China Inf. Sci. 60 (7) (Jul 2017) 070201, https://doi.org/10.1007/s11432-016-9088-2.
[2] C. Yuan, Z. Liu, Y. Zhang, Learning-based smoke detection for unmanned aerial vehicles applied to forest fire surveillance, J. Intell. Robot. Syst. 93 (1–2) (2018) 337–349, https://doi.org/10.1007/s10846-018-0803-y.
[3] Y. Liu, H. Liu, Y. Tian, C. Sun, Reinforcement learning based two-level control framework of UAV swarm for cooperative persistent surveillance in an unknown urban area, Aerosp. Sci. Technol. 98 (2020), https://doi.org/10.1016/j.ast.2019.105671.
[4] Q. Sheng, Y. Zhang, Z. Zhu, W. Li, J. Xu, R. Tang, An experimental study to quantify road greenbelts and their association with PM2.5 concentration along city main roads in Nanjing, China, Sci. Total Environ. 667 (Jun 1 2019) 710–717, https://doi.org/10.1016/j.scitotenv.2019.02.306.
[5] B. Shirani, M. Najafi, I. Izadi, Cooperative load transportation using multiple UAVs, Aerosp. Sci. Technol. 84 (2019) 158–169, https://doi.org/10.1016/j.ast.2018.10.027.
[6] Z. Zhen, Y. Chen, L. Wen, B. Han, An intelligent cooperative mission planning scheme of UAV swarm in uncertain dynamic environment, Aerosp. Sci. Technol. 100 (2020), https://doi.org/10.1016/j.ast.2020.105826.
[7] M. Lu, L. Liu, Leader–following consensus of multiple uncertain Euler–Lagrange systems with unknown dynamic leader, IEEE Trans. Autom. Control 64 (10) (2019) 4167–4173, https://doi.org/10.1109/tac.2019.2892384.
[8] J. Yu, X. Dong, Q. Li, Z. Ren, Distributed cooperative encirclement hunting guidance for multiple flight vehicles system, Aerosp. Sci. Technol. 95 (2019), https://doi.org/10.1016/j.ast.2019.105475.
[9] L.C.A. Pimenta, et al., Swarm coordination based on smoothed particle hydrodynamics technique, IEEE Trans. Robot. 29 (2) (Apr 2013) 383–399, https://doi.org/10.1109/Tro.2012.2234294.
[10] Y. Xu, D. Luo, H. Duan, Distributed planar formation maneuvering of leader-follower networked systems via a barycentric coordinate-based approach, Sci. China, Technol. Sci. 64 (8) (2021) 1705–1718, https://doi.org/10.1007/s11431-020-1797-5.

[11] L. Li, P. Shi, R.K. Agarwal, C.K. Ahn, W. Xing, Event-triggered model predictive control for multiagent systems with communication constraints, IEEE Trans. Syst. Man Cybern. Syst. 51 (5) (2021) 3304–3316, https://doi.org/10.1109/tsmc.2019.2932838.
[12] Y. Cai, H. Zhang, Y. Wang, J. Zhang, Q. He, Fixed-time time-varying formation tracking for nonlinear multi-agent systems under event-triggered mechanism, Inf. Sci. 564 (2021) 45–70, https://doi.org/10.1016/j.ins.2021.02.071.
[13] M. Huo, H. Duan, X. Ding, Manned aircraft and unmanned aerial vehicle heterogeneous formation flight control via heterogeneous pigeon flock consistency, Unmanned Syst. 09 (03) (2021) 227–236, https://doi.org/10.1142/s2301385021410053.
[14] M. Huo, H. Duan, Y. Fan, Pigeon-inspired circular formation control for multi-UAV system with limited target information, Guid. Navig. Control 01 (01) (2021), https://doi.org/10.1142/s2737480721500047.
[15] Z.A. Ali, Z.G. Han, Multi-unmanned aerial vehicle swarm formation control using hybrid strategy, Trans. Inst. Meas. Control 43 (12) (Aug 2021) 2689–2701, https://doi.org/10.1177/01423312211003807.
[16] M. Shafiq, Z.A. Ali, E.H. Alkhammash, A cluster-based hierarchical-approach for the path planning of swarm, Appl. Sci. 11 (15) (2021), https://doi.org/10.3390/app11156864.
[17] Z.A. Ali, Z. Han, R.J. Masood, Collective motion and self-organization of a swarm of UAVs: a cluster-based architecture, Sensors 21 (11) (May 31 2021), https://doi.org/10.3390/s21113820.
[18] H. Cai, F.L. Lewis, G. Hu, J. Huang, The adaptive distributed observer approach to the cooperative output regulation of linear multi-agent systems, Automatica 75 (2017) 299–305, https://doi.org/10.1016/j.automatica.2016.09.038.
[19] W. Perruquetti, T. Floquet, E. Moulay, Finite-time observers: application to secure communication, IEEE Trans. Autom. Control 53 (1) (2008) 356–360, https://doi.org/10.1109/tac.2007.914264.
[20] M. Zhang, Y. Shen, Q.A. Wang, Y.B. Wang, Dynamic artificial potential field based multi-robot formation control, in: 2010 IEEE International Instrumentation and Measurement Technology Conference 2010, Proceedings, June 2010.
[21] Z. Cai, H. Zhou, J. Zhao, K. Wu, Y. Wang, Formation control of multiple unmanned aerial vehicles by event-triggered distributed model predictive control, IEEE Access 6 (2018) 55614–55627, https://doi.org/10.1109/access.2018.2872529.
[22] Z. Yu, et al., Nussbaum-based finite-time fractional-order backstepping fault-tolerant flight control of fixed-wing UAV against input saturation with hardware-in-the-loop validation, Mech. Syst. Signal Process. 153 (2021), https://doi.org/10.1016/j.ymssp.2020.107406.
[23] Q. Hu, X. Shao, Y. Zhang, L. Guo, Nussbaum-type function-based attitude control of spacecraft with actuator saturation, Int. J. Robust Nonlinear Control 28 (8) (2018) 2927–2949, https://doi.org/10.1002/rnc.4056.
[24] Z. Yu, Z. Liu, Y. Zhang, Y. Qu, C.Y. Su, Distributed finite-time fault-tolerant containment control for multiple unmanned aerial vehicles, IEEE Trans. Neural Netw. Learn. Syst. 31 (6) (Jun 2020) 2077–2091, https://doi.org/10.1109/TNNLS.2019.2927887.
[25] Z.Q. Yu, Y.H. Qu, Y.M. Zhang, Distributed fault-tolerant cooperative control for multi-UAVs under actuator fault and input saturation, IEEE Trans. Control Syst. Technol. 27 (6) (Nov 2019) 2417–2429, https://doi.org/10.1109/Tcst.2018.2868038.
[26] Z.Q. Yu, Y.M. Zhang, Y.H. Qu, Prescribed performance-based distributed fault-tolerant cooperative control for multi-UAVs, Trans. Inst. Meas. Control 41 (4) (Feb 2019) 975–989, https://doi.org/10.1177/0142331218809006.
[27] X. Shao, Q. Hu, Y. Shi, B. Jiang, Fault-tolerant prescribed performance attitude tracking control for spacecraft under input saturation, IEEE Trans. Control Syst. Technol. 28 (2) (2020) 574–582, https://doi.org/10.1109/tcst.2018.2875426.
[28] J.L. Ma, S.Y. Xu, G.M. Zhuang, Y.L. Wei, Z.Q. Zhang, Adaptive neural network tracking control for uncertain nonlinear systems with input delay and saturation, Int. J. Robust Nonlinear Control 30 (7) (May 10 2020) 2593–2610, https://doi.org/10.1002/rnc.4887.
[29] G. Zhu, J. Du, Robust adaptive neural practical fixed-time tracking control for uncertain Euler-Lagrange systems under input saturations, Neurocomputing 412 (2020) 502–513, https://doi.org/10.1016/j.neucom.2020.05.057.
[30] S. Zhao, Y. Pan, P. Du, H. Liang, Adaptive control for non-affine nonlinear systems with input saturation and output dead zone, Appl. Math. Comput. 386 (2020), https://doi.org/10.1016/j.amc.2020.125506.
[31] L. Ma, G. Zong, X. Zhao, X. Huo, Observed-based adaptive finite-time tracking control for a class of nonstrict-feedback nonlinear systems with input saturation, J. Franklin Inst. 357 (16) (2020) 11518–11544, https://doi.org/10.1016/j.jfranklin.2019.07.021.
[32] G.B. Zhu, J.L. Du, Global robust adaptive trajectory tracking control for surface ships under input saturation, IEEE J. Ocean. Eng. 45 (2) (Apr 2020) 442–450, https://doi.org/10.1109/Joe.2018.2877895.
[33] J. Yu, P. Shi, C. Lin, H. Yu, Adaptive neural command filtering control for nonlinear MIMO systems with saturation input and unknown control direction, IEEE Trans. Cybern. 50 (6) (Jun 2020) 2536–2545, https://doi.org/10.1109/TCYB.2019.2901250.
[34] S. Li, X. Wang, Finite-time consensus and collision avoidance control algorithms for multiple AUVs, Automatica 49 (11) (2013) 3359–3367, https://doi.org/10.1016/j.automatica.2013.08.003.
[35] Z. Zhen, D. Xing, C. Gao, Cooperative search-attack mission planning for multi-UAV based on intelligent self-organized algorithm, Aerosp. Sci. Technol. 76 (2018) 402–411, https://doi.org/10.1016/j.ast.2018.01.035.
[36] Y. Liu, R. Bucknall, A survey of formation control and motion planning of multiple unmanned vehicles, Robotica 36 (7) (2018) 1019–1047, https://doi.org/10.1017/s0263574718000218.
[37] Q. Li, J. Wei, Q. Gou, Z. Niu, Distributed adaptive fixed-time formation control for second-order multi-agent systems with collision avoidance, Inf. Sci. 564 (2021) 27–44, https://doi.org/10.1016/j.ins.2021.02.029.
[38] S.-S. Ge, X. Liu, C. Goh, L. Xu, Formation tracking control of multiagents in constrained space, IEEE Trans. Control Syst. Technol. 24 (3) (2016) 992–1003, https//doi.org/10.1109/tcst.2015.2472959.
[39] Zhang Zhongnan, Ling Qing, Y. Zaiyue, Formation control with obstacle avoidance of multi-robot systems with second-order dynamics, in: 2019 38th Chinese Control Conference (CCC), 2019.
[40] F. Mehdifar, C.P. Bechlioulis, F. Hashemzadeh, M. Baradarannia, Prescribed performance distance-based formation control of Multi-Agent Systems, Automatica 119 (2020), https://doi.org/10.1016/j.automatica.2020.109086.
[41] S.-L. Dai, S. He, X. Chen, X. Jin, Adaptive leader–follower formation control of nonholonomic mobile robots with prescribed transient and steady-state performance, IEEE Trans. Ind. Inform. 16 (6) (2020) 3662–3671, https://doi.org/10.1109/tii.2019.2939263.
[42] B.S. Park, S.J. Yoo, Adaptive-observer-based formation tracking of networked uncertain underactuated surface vessels with connectivity preservation and collision avoidance, J. Franklin Inst. 356 (15) (2019) 7947–7966, https://doi.org/10.1016/j.jfranklin.2019.04.017.
[43] X. Fu, J. Pan, H. Wang, X. Gao, A formation maintenance and reconstruction method of UAV swarm based on distributed control, Aerosp. Sci. Technol. 104 (2020) 105981, https://doi.org/10.1016/j.ast.2020.105981.
[44] A.-M. Zou, Z.-G. Hou, M. Tan, Adaptive control of a class of nonlinear pure-feedback systems using fuzzy backstepping approach, IEEE Trans. Fuzzy Syst. 16 (4) (2008) 886–897, https://doi.org/10.1109/tfuzz.2008.917301.
[45] D.D. Mu, G.F. Wang, Y.S. Fan, Tracking control of podded propulsion unmanned surface vehicle with unknown dynamics and disturbance under input saturation, Int. J. Control. Autom. Syst. 16 (4) (2018) 1905–1915, https://doi.org/10.1007/s12555-017-0292-y.
[46] Z. Yu, Y. Zhang, B. Jiang, C.-Y. Su, J. Fu, Y. Jin, T. Chai, Decentralized fractional-order backstepping fault-tolerant control of multi-UAVs against actuator faults and wind effects, Aerosp. Sci. Technol. 104 (2020) 105939, https://doi.org/10.1016/j.ast.2020.105939.
[47] M.V. Basin, P. Yu, Y.B. Shtessel, Hypersonic missile adaptive sliding mode control using finite- and fixed-time observers, IEEE Trans. Ind. Electron. 65 (1) (2018) 930–941, https://doi.org/10.1109/tie.2017.2701776.